Testing for ocean acidification during the Early Toarcian using $\delta^{44/40}$Ca and $\delta^{88/86}$Sr.

Q. Li [1*], J.M. McArthur [1, 2#], M.F. Thirlwall [1], A.V. Turchyn [3], K. Page [4], H.J. Bradbury [3], R. Weis [5] and D. Lowry [1]

1. Earth Science, Royal Holloway University of London, Egham Hill, Egham, UK, TW20 0EX
2. Department of Earth Sciences, UCL, Gower Street, London WC1E 6BT, UK
3. Department of Earth Sciences, University of Cambridge, Cambridge, UK
4. University of Exeter, Penryn Campus, Penryn, Cornwall TR10 9FE,UK.
5. Palaeontological Department, National Museum of Natural History, 25 rue Münster, L-2160, Luxembourg, Grand-duchy of Luxembourg.

**Present address, Nu Instruments, Clywedog Road South, Wrexham, UK, LL13 9XS*
 # Corresponding author email: j.mcarthur@ucl.ac.uk

Abstract

During the early Toarcian, volcanic gases released by the Karoo-Ferrar large igneous province are widely believed to have caused severe environmental disturbances, including ocean acidification. Here we show records of $\delta^{44/40}$Ca and $\delta^{88/86}$Sr through the early Toarcian, as recorded in three groups of biogenic calcite: Megateuthididae belemnites, Passaloteuthididae belemnites, and brachiopods of the species *Soaresirhynchia bouchardi*. We evaluate the data to eliminate the influence on isotopic composition of varying temperature, calcification rate, and salinity, through the section that may mask the environmental signals.

Neither $\delta^{44/40}$Ca and $\delta^{88/86}$Sr show negative isotope excursions across the suggested acidification interval as would be expected had acidification occurred. A profile of δ^{11}B, re-interpreted from a published study, shows no variation through the interval. Taken together, these data provide little support for ocean acidification at this time.

Values of $\delta^{88/86}$Sr are independent of temperature or Sr/Ca in our belemnites. For brachiopods, too few data are available to determine whether such a dependence exists. Values of $\delta^{44/40}$Ca show a weak temperature control of magnitude $+0.020 \pm 0.004$ ‰/°C (2s.d.). In belemnites, $\delta^{44/40}$Ca also correlates positively with Mg/Ca and Sr/Ca.

Keywords: Ca-isotopes, Sr-isotopes, Toarcian, OAE, ocean acidification.

1. Introduction

The three million years between the late Pliensbachian and the early Toarcian (185 to around 182 Ma; Gradstein *et al.* 2020) was an interval of biotic change (Hallam 1986; Raup and Sepkoski 1986; Little and Benton 1995; Harries and Little 1999; Caswell *et al.* 2009; Danise *et al.* 2013). Although often termed a time of mass extinction (Little and Benton 1995), the biotic turnover was minor in comparison to the five most severe extinctions of the Phanerozoic and extended over 5 (Little and Benton 1995) or 7 (Dera *et al.* 2010) ammonite Zones.

In the interval, large variations occurred in the isotopic composition of inorganic and organic carbon (Küspert 1982; Hesselbo *et al.* 2000, 2007, McArthur 2007, van de Schootbrugge *et al.* 2013; Suan *et al.* 2015; Bodin *et al.* 2016; Xu *et al.* 2018). In the early Toarcian, large temperature fluctuations are recorded in $\delta^{18}O$ of biogenic calcite (Bailey *et al.* 2003; Suan *et al.* 2008, 2010) together with a diminution of carbonate production (Suan *et al.* 2008, Mattioli *et al.* 2009; Trecalli *et al.* 2012; Krencker *et al.* 2020). Organic-rich sediments were deposited in several marginal basins around the world *e.g.* in NW Europe (Jenkyns 1988), ~~Argentina (Al Suwaidi *et al.* 2009),~~ Japan (Kemp and Izumi 2014), and China (Xu *et al.* 2017) whilst organic-poor sediments were deposited elsewhere *e.g.* Peniche (Hesselbo *et al.* 2007) and Morocco (Bodin *et al.* 2010, 2016). Substantial variations occurred in time, and between localities, in the isotopic composition of molybdenum (Pearce *et al.* 2008; Dickson *et al.* 2017) and osmium (Cohen *et al.* 2004; van Acken *et al.* 2019) in the basins of NW Europe, probably in response to hydrographic restriction (Küspert 1982, Saelen *et al.* 1996; McArthur 2019).

The environmental perturbations listed above are commonly attributed to the effects of LIP volcanism *i.e.* the Karoo-Ferrar large igneous province (Pálfy and Smith 2000; Burgess *et al.* 2015; Percival *et al.* 2016; many others) because radiometric dating places much of the eruptive phase of this volcanism in the late Pliensbachian through early Toarcian (Jourdan *et al.* 2005, 2007, 2008; Burgess *et al.* 2015, Ivanov *et al.* 2017; Moulin *et al.* 2017). Copious amounts of CO_2, HCl, HF, and SO_2, may have been emitted by Karoo-Ferrar volcanism (Black *et al.* 2012; Schmidt *et al.* 2016, Jones *et al.* 2016). Dissolution of such gases in seawater might have caused ocean acidification: isotope excursions in $\delta^{44}Ca$ (Brazier *et al.* 2015) and $\delta^{11}B$ (Müller *et al.* 2020) and the demise of some carbonate platforms (*e.g.* Trecalli *et al.* 2012; Ettinger *et al.* 2021) appear to support this view.

Marine carbonates are isotopically less positive than seawater in both $\delta^{44/40}Ca$ (Skulan *et al.* 1997) and $\delta^{88/86}Sr$ (Fietzke and Eisenhauer 2006) through preferential incorporation of ^{40}Ca over ^{44}Ca and ^{86}Sr over ^{88}Sr. The isotopic compositions of Ca and Sr in seawater are therefore enriched in the heavier isotopes relative to carbonate sediments. Ocean acidification, by decreasing carbonate sedimentation and/or dissolving existing carbonate sediments, adds isotopically lighter Ca and Sr isotopes to the ocean and so generates, or contributes to, negative excursions of both $\delta^{44/40}Ca$ and

$\delta^{88/86}$Sr in seawater, such as those of up to 0.6 ‰ in $\delta^{44/40}$Ca across the Permian-Triassic boundary (Payne *et al.* 2010; Hinojosa *et al.* 2012; Silva-Tamayo *et al.* 2018) and the negative excursions of 0.8 ‰ in $\delta^{44/40}$Ca across the Triassic-Jurassic boundary (Jost *et al.* 2017), of which 20% (0.16‰) is attributed by those authors to ocean acidification. In contrast, no negative shift in $\delta^{44/40}$Ca is seen across the Paleocene-Eocene Thermal Maximum (Site 1212B of Griffith *et al.*, 2015), a time when ocean acidification is thought to have occurred (*e.g.* Penman *et al.* 2014)

Here, we report $\delta^{44/40}$Ca and $\delta^{88/86}$Sr in belemnite and brachiopod carbonate through a composite section spanning Early Toarcian time in order to look for isotopic indicators of ocean acidification in that interval and also to contribute towards defining the secular evolution of the Ca- and Sr-isotopic composition of seawater through Phanerozoic time.

2. Study Areas and Samples

2.1. Stratigraphy

Our samples come Yorkshire, UK, and Peniche, Portugal (Fig. 1). The stratigraphy of both sections is summarized in Fig. 2, along with profiles of C-isotope variations through the sections.

The coastal sections at Peniche expose hemipelagic coccolith-bearing marls and limestones of the Lemede and Cabo Carvoeiro Formations, of Late Pliensbachian and Early Toarcian age. Ammonite biostratigraphy for Peniche was first recorded by Mouterde (1955, 1967) and updated by Elmi (2006, 2007); Rocha *et al.* (2016), Duarte *et al.* (2017) and Duarte *et al.* (2018). The lowermost Toarcian zone, the Tenuicostatum Zone, comprises a lower *mirabile* Subzone that is 0.2 m thick and is overlain by an upper *semicelatum II* Subzone that is 11 m thick. The overlying Falciferum Zone at Peniche has no formal subzones. The base of the Toarcian is at the base of the Bed 15e, the uppermost bed of the Lemede Formation. Peniche is the GSSP for the Toarcian Stage, despite contravening several of the requirements for such a choice, notably regarding the completeness of the section (McArthur *et al.* 2020; Supplementary Information). Bed 15e, some 20cm thick, encompasses the entire *mirabile* Subzone and is highly condensed. The condensation diminishes upward but extends some 3 m above the boundary (ibid.). An hiatus marks the base of the Falciferum Zone (Pittet *et al.* 2014).

Coastal sections in Yorkshire, UK, expose shales deposited in the Cleveland Basin. The lithology and ammonite zonation of the sediments of Toarcian age given in Howarth (1962, 1991), whose bed numbers are used here. The same ammonite zones are recognised in Peniche and Yorkshire (Page 2004; McArthur *et al.* 2020). In Yorkshire, the Falciferum Zone is divided into a lower *exaratum* Subzone and an overlying *falciferum* Subzone. The *exaratum* Sz. coincides with a lithological unit originally known as the Jet Rock, now renamed the lower part of the Mulgrave Shale Member of the Whitby Mudstone Formation. The interval from the uppermost *semicelatum I*

Subzone (middle of Bed 31) to the top of the overlying *exaratum* Subzone (base of bed 41) may encompass an oceanic anoxic event (Jenkyns 1988 *et seq.*) or be one example of regional anoxia in marginal basins (McArthur *et al.* 2008, McArthur 2019). The middle part of this interval is organic-rich with concentrations of total organic carbon reaching 18% (McArthur *et al.* 2008).

2.2. Environments

Peniche and Yorkshire show similar stratigraphic trends in their carbon-isotope composition, with an interval of lower values between positive excursions in $\delta^{13}C$ at the top and bottom of the interval (Fig. 2). Between the positive excursions, the full stratigraphic development of which outside the range of Fig. 2, values of $\delta^{13}C$ in belemnite calcite is around +1‰, a value typical of most of Mesozoic time. Values of $\delta^{13}C$ in bulk sediment closely track the trend in macrofossil $\delta^{13}C$ but around 1‰ less positive. Previous studies (*e.g.* Röhl *et al.* 2001; Wignall *et al.* 2005) have documented the fact that changes in $\delta^{13}C$ through the section occurred in parallel with changes in redox conditions of the water column in Yorkshire, allowing three intervals of differing redox conditions in the water column to be identified (Fig. 2), although their strict application to Peniche may not be appropriate – see Fantasia *et al.* (2019) and the discussion below.

In Interval 1, the water column at both localities appears to have been oxic (benthic faunas are present) and values of $\delta^{13}C_{org}$ are around −25 ‰. Values of $\delta^{13}C_{carb}$ rise to a peak of around 2.5 ‰ and form the rising limb of a positive excursion of around +2.5 ‰ in the Tenuicostatum Zone that occurs widely elsewhere (Harazim *et al.* 2013; Bodin *et al.* 2016).

Interval 2 marked a decline in oxygenation of the water column that began in Yorkshire in the upper part of the *Semicelatum I* Subzone and developed into mostly euxinic conditions during *exaratum* times, the euxinia extending into the photic zone as shown by decreases in the size of framboidal pyrite in sediments (Wignall *et al.* 2005) and the presence in sediments of molecular biomarkers for photic-zone euxinia (Fig. 2; Schouten *et al.* 2000; French *et al.* 2014). Brief periods of oxygenation were recorded by short-lived invasions of benthos (*e.g.* Caswell *et al.* 2009, Caswell and Coe, 2013). In Peniche, development of such conditions was more subdued but may have occurred over the same interval. Upwards from the mid-Tenuicostatum Zone, the carbonate content of the sediment declined, nanno-plankton showed increasing signs of stress (Suan *et al.* 2008) and belemnites became scarcer and smaller. The positive excursion in $\delta^{13}C_{carb}$ peaked in the mid-Tenuicostatum Zone and trends to less positive values in the interval from 8 m to 12 m above datum. The paucity of benthic faunas between 11 and 21 m in the section suggests that the bottom water in Peniche were dysoxic, although Fantasia *et al.* (2019) argue for normally oxygenated bottom waters in this interval. Traces of dolomite are found throughout the section but are more common (2–3 % of the sediment) between 11 and 21 m (Hermoso 2009).

In Interval 3, the force driving unfavourable conditions in the water column(s?) retreated and values of $\delta^{13}C$ increased in both localities to define the well-known positive isotope excursion that was for some time the recognised marker for the putative Early Toarcian oceanic anoxic event. Benthic faunas returned in Peniche at the start of Interval 3 but euxinia persisted into the upper part of the *exaratum* Subzone in Yorkshire. Our brachiopod samples from Peniche were therefore alive during the euxinic interval in Yorkshire.

The Cleveland Basin, Yorkshire, the source of the Yorkshire belemnites, was hydrographically restricted for much, if not most, of *exaratum* time (McArthur *et al.* 2008; McArthur 2019), with euxinia extending into the photic zone (Schouten *et al.,* 2000; Wignall *et al.,* 2005; French *et al.* 2014). Nevertheless, ammonite faunas preserved in sediments of the *exaratum* Subzone in Yorkshire attest to an oxic surface layer, at least at times. Sporadic benthic colonisation in the *exaratum* Sz. of Yorkshire (Caswell *et al.* 2009; Caswell and Coe 2013) and in the temporally-equivalent Posidonia Shale in Germany (Röhl *et al.* 2001; Schmid-Röhl *et al.* 2002) by opportunistic bivalves testify to multiple oxygenation events affecting the entire water column, events possibly as brief as a single season (*ibid*). The Yorkshire belemnites record temperatures higher than samples from Peniche, but appear otherwise typical of Jurassic belemnites. The $^{87}Sr/^{86}Sr$ ratios of specimens from both localities are concordant (McArthur *et al.* 2020) and the values of $\delta^{13}C$, Mg/Ca, and Sr/Ca in the Yorkshire belemnites are not obviously anomalous in comparison to belemnites from upper Pliensbachian and lower Toarcian strata at Peniche and elsewhere *e.g.* Spain (Rosales *et al.* 2004).

3. Sample preparation and analysis

3.1. Samples

Samples from Peniche were mostly belemnites of the family Passaloteuthididae, but the two stratigraphically highest, from Bed 133 at 35 m, are of the family Megateuthididae. The samples are a subset of those used to derive an $^{87}Sr/^{86}Sr$ profile through the section in Peniche (McArthur et al. 2020). We also analysed four specimens of the brachiopod *Soaresirhynchia bouchardi*. No macrofossils were found between 11 m and 19 m in the section at Peniche. We filled this stratigraphic gap with six belemnites from the correlative Whitby Mudstone Formation, Yorkshire, UK.

Of the Yorkshire samples, two (PM 13, PM 106) were used in McArthur *et al.* (2000) and four were newly collected. Two belemnites derive from the uppermost part of Bed 32, in the uppermost *semicelatum I* Subzone, 20 – 40 cm below the base of the *exaratum* Subzone. Three belemnites are from the *exaratum* Subzone (Beds 34, 35, 38, of Howarth 1962). The sixth was collected 10 cm above the *exaratum* Sz. and so 10 cm above the base of Bed 41. The lowest of the Yorkshire belemnites, from the upper part of Bed 32, belongs to the family Passaloteuthididae whilst the remainder are of the family Megateuthididae (Table 1).

3.2 Preparation

For belemnites, the exterior, the apical line, and other visually altered areas, were removed using diamond cutting tools. The samples were then broken into pieces and a piece of the stem region of the rostrum was crushed in an agate pestle-and-mortar. The fragments were immersed briefly (≈ 3 seconds) in 1.2 M hydrochloric acid to remove calcite fines, rinsed with 18 MΩ water, and dried in a clean-hood. For analysis, fragments of mm or smaller size were picked from a methanol bath under the binocular microscope. Brachiopods were trimmed of adhering sediment using a scalpel and then gently crushed. Clean flakes of the fibrous calcite from the secondary (inner) shell were picked under the microscope for analysis. Analyzed fragments comprised translucent uncoloured calcite. Analyzed fragments were judged to be sufficiently well-preserved to retain their original compositions and isotopic signatures without material alteration. Each type of analysis (Ca-, C/O-, Sr-isotope; elemental) used different picked subsamples. Details of state of preservation are given in the Supplementary Information, including photomicrographs of analyzed sampled (Fig. S1) and major and trace-element composition is given in Table 1.

3.3. Measurements of $\delta^{44/40}$Ca

Twenty-three samples were measured on a Triton Plus Thermal ionization mass spectrometer (TIMS) at the University of Cambridge following the procedures in Bradbury and Turchyn (2018) using a ^{42}Ca – ^{48}Ca-isotope double spike. Seven samples were measured on a IsotopX Phoenix-X62 TIMS at Royal Holloway University of London (RHUL) broadly following the procedures of Li *et al.* (2016) using a ^{43}Ca – ^{46}Ca-isotope double spike. Full details of the procedures are given in the Supplementary Information. No column separation was performed on samples or standards before analysis for Ca-isotopes. The results of our analysis are given in Table 1. We report $\delta^{44/40}$Ca relative to SRM915a. At Cambridge, replicate measurements of NIST SRM-915b standard yield an average of 0.76 ± 0.12 ‰ (2sd, n = 29) on $\delta^{44}/^{40}$Ca, relative to SRM-915a. At RHUL, analyses of HPS_{new} yielded a mean $\delta^{44}/^{40}$Ca value of 0.71 ± 0.20 ‰ (2 s.d. n = 11) relative to SRM-915a, consistent with its published values (Reynard et al., 2010 and Li et al., 2016).

3.4. Measurement of $\delta^{88/86}$Sr

Strontium isotope analyses were performed on the IsotopX Phoenix-X62 TIMS at Royal Holloway University of London (RHUL). An ^{87}Sr - ^{84}Sr double spike solution was used to correct for mass fractionation and to determine the true Sr isotope ratios of samples. Spiked and unspiked samples were prepared and run separately for $\delta^{88/86}Sr$ and $^{87}Sr/^{86}Sr$ analysis. Further details of analytical methods are given in the Supplementary Information. During the course of the analysis, SRM 987 and IAPSO seawater were analysed as primary and secondary standards to monitor the performance of Sr measurements and to check the accuracy of the double spike correction method. Measurements of SRM 987 yield an average $^{84}Sr/^{86}Sr$ of 0.056487 ± 0.000009 (internally normalised to $^{86}Sr/^{88}Sr$ of 0.1194) , and a mean $^{87}Sr/^{86}Sr$ of 0.710239 ± 0.000009 (also normalised to 0.1194). The mean $\delta^{88/86}Sr$ of IAPSO seawater measured during this study was 0.390 ± 0.009 ‰ (2.s.e., n = 20), consistent with the published value of 0.386 ± 0.010 (2.s.e., n = 10; Krabbenhöft *et al.* 2009). The analytical uncertainty of the measurements at 2s.d. is ± 0.04 ‰. The results of our analysis are given in Table. 1.

3.5. Measurement of $\delta^{13}C$ and $\delta^{18}O$ and elemental composition

Analysis of calcite for $\delta^{13}C$ and $\delta^{18}O$ was done at RHUL using a GV Instruments (now Elementar) Multiflow preparation system on line to an IsoPrime mass spectrometer. Standards used were NBS 19 and LSVEC international standards and RHUL internal calcite standard. External precision (2s.d.) of standards during the period of sample analysis was ≤ ± 0.05 ‰ for $\delta^{13}C$ and ≤ ± 0.10 ‰ for $\delta^{18}O$. At UCL, analysis of calcite for $\delta^{13}C$ and $\delta^{18}O$ was undertaken with a Thermo Delta Plus XP mass spectrometer attached to a Thermo Gas Bench II device and a CTC Pal auto-sampler. Calibration was with in-house standard and NBS 19. External precision (2s.d.) of standards during the period of sample analysis was ≤ 0.04 ‰ for $\delta^{13}C$ and ≤ 0.10 ‰ for $\delta^{18}O$.

To measure elemental composition, samples of 10 ± 0.2 mg were dissolved overnight in 10 ml of 1.2% nitric acid and were analysed for Ca, Ba, Fe, and Mn by direct comparison of intensities to the intensities of commercial standards (VWR®) matrix-matched to samples. Analysis was undertaken with a Varian 720 ICP-OES. Using a separate set of matrix-matched standards, values of Mg/Ca and Sr/Ca only were obtained by the intensity-ratio method of de Villiers (2002) and used to calculate Sr and Mg values from measured Ca.

3.6. Isotopic fractionation of $\delta^{44/40}Ca$

We seek to define the variations through time in the $\delta^{44/40}Ca$ of seawater, so factors affecting the fractionation of Ca-isotopes into marine biogenic calcite must be corrected for. These factors are mineralogy (aragonite *v* calcite), taxonomic group/vital effects (fractionation factors for belemnites differ from those for brachiopods, Gussone *et al.* 2005; Farkaš *et al.* 2007a), temperature (*e.g.* Nägler *et al.* 2000; von Allmen *et al.* 2010; Gussone & Heuser 2016), and kinetics/rate of calcification (Kisakürek *et al.* 2011). The original mineralogy of the brachiopods, and the belemnite rostra, we have analysed was calcite, so there is no mineralogical control on our data. We correct for other controls as follows.

Taxonomic group: to account for the fact that we have analysed belemnites and brachiopods, we convert from measured $\delta^{44/40}Ca_{cal}$ to what we term here base-$\delta^{44/40}Ca_{cal}$ using fractionations of 1.4 ‰ for belemnites (Farkaš *et al.* 2007a) and 0.85 ‰ for brachiopods (Gussone *et al.* 2005). This process converts $\delta^{44/40}Ca_{cal}$ to a value that approximates the $\delta^{44/40}Ca$ of the fluid from which they precipitate, which in this case is the $\delta^{44/40}Ca$ of seawater; the values are approximate as they are, at this point, not corrected for the effects on $^{44/40}Ca$ of different temperatures and calcification rates between specimens – see next two sections.

Temperature: Temperatures were derived from $\delta^{18}O$ (Table 1) using the palaeo-temperature equation of Hays and Grossman (1991), and a value of −1 ‰ for $\delta^{18}O_{sw}$. We correct base-$\delta^{44/40}Ca_{cal}$ to a common temperature of 15° C using a temperature dependence of Ca-isotope fractionation of +0.020 ‰/°C derived from the slope of the regression line between temperature and $\delta^{44/40}Ca$ (Fig. 3a). We use the term temperature-corrected-$\delta^{44/40}Ca_{cal}$ for the result. Both brachiopods and belemnites fall on the regression line in Fig. 3a. The temperature dependency of +0.020 ± 0.004 ‰/°C (2s.d., $n = 44$) is similar in magnitude and sign to that reported by others (*e.g.* Gussone and Heuser 2016; but see also Farkaš *et al.* 2007a,b).

The positive correlation between base-$\delta^{44/40}Ca_{cal}$ and temperature (Fig. 3a) might be interpreted as suggesting that the isotopic composition of oxygen in belemnites is controlled by kinetic, not equilibrium, isotope fractionation (McConnaughey 1989; Watkins *et al.* 2013; Daëron *et al.* 2019). Kinetic control is unlikely given the demonstration by Bajnai *et al.* (2020) that belemnites grew in isotopic equilibrium with ambient water. Furthermore, values of $\delta^{18}O$ do not correlate with $\delta^{13}C$ (Fig. S2, Supplementary Information; see also Uchikawa and Zeebe 2012), so we conclude that kinetics are at most a minor control on belemnite composition, probably contributing only to the scatter of data about the regression line in Fig. 3a.

Calcification rate: in the analysed belemnites, base-$\delta^{44/40}Ca_{cal}$ correlates positively with Mg/Ca and Sr/Ca (Fig. 3b, c). A strong inverse relation between $\delta^{44/40}Ca_{cal}$ and Sr/Ca in inorganic calcite was found experimentally by Tang (2008) and ascribed to kinetic isotope fractionation governed by precipitation (calcification) rate. Modelling and measurement has subsequently confirmed these findings (DePaolo 2011; Nielsen *et al*. 2012). The absence in our samples of an inverse correlation between $\delta^{44/40}Ca_{cal}$ and Sr/Ca shows either that the results of inorganic experiments must be applied with caution to biogenic calcite or that calcification rate has only a minor influence on $\delta^{44/40}Ca$ in our samples. The latter deduction agrees with the observation of Ullmann and Pogge von Strandmann (2017) that, for a single specimen of *Passaloteuthis bisulcata* (Blainville, 1827), calcification-rate affected Mg/Ca minimally, with Mg/Ca *decreasing* by around 8% for a doubling of growth rate.

Temperature is the main control on both Mg/Ca and $\delta^{44/40}$Ca, so the correlation between these two variables (Fig. 3b) might be viewed as simply induced and reflects that master control on both. It is therefore odd that, for belemnites, values of Mg/Ca correlate with base-$\delta^{44/40}Ca_{cal}$ (Fig. 3b, r = 0.89) more strongly than do temperatures (r = 0.82, not shown) and more strongly than the temperature correlates with $\delta^{44/40}$Ca for the entire data set (Fig. 3a, r = 0.81). The better correlation of base-δ^{44}Ca with Mg/Ca (Fig. 3b) over the correlation of base-δ^{44}Ca with temperature (Fig. 3a) implies that base-$\delta^{44/40}Ca_{cal}$ in belemnites might be *marginally* influenced by kinetic factors *i.e.* variations in calcification rate, and that the marginal difference between correlation coefficients in Fig 3a and Fig. 3b reflects that additional but marginal influence. If so, correcting values of δ^{44}Ca to a common value of Mg/Ca, rather than to a common temperature, will give values of $\delta^{44/40}$Ca that better reflect ambient seawater values. In addition to correcting for temperature, we therefore separately also correct base-$\delta^{44/40}Ca_{cal}$ to a common Mg/Ca of 11.5 mM/M using the slope of the correlation line in Fig. 3b ($\Delta\delta^{44/40}$Ca/ΔMg/Ca of 0.045 ‰/mM/M). The term detrended-$\delta^{44/40}Ca_{cal}$ is applied to the result. The value of 11.5 does not represent the Mg/Ca of Early Toarcian seawater; the number is a convention adopted to bring all data to a common baseline. We use 11.5 because it is the middle value of the range of Mg/Ca of the samples; its use therefore minimizes changes to $\delta^{44/40}Ca_{cal}$. Other values could be used but with essentially similar results – to bring values of Mg/Ca to a common baseline. The correction does not apply to the brachiopods, so brachiopods are omitted from consideration when detrended-$\delta^{44/40}Ca_{cal}$ is discussed in later sections.

3.7. Isotopic fractionation of $\delta^{88/86}$Sr

We seek to define the variations through time in the $\delta^{88/86}$Sr of seawater, so factors affecting the fractionation of Sr isotopes into marine biogenic calcite must be corrected for. These factors are temperature, taxonomic group, rate of precipitation and (possibly) mineralogy *i.e.* aragonite *v* calcite (Fietzke and Eisenhauer 2006; Böhm *et al.* 2012; Vollstaedt *et al.* 2014; Al-Khatib and Eisenhauer 2017). As we analysed only calcite, a mineralogical control is absent.

Taxonomic group: we can identify no taxonomic effect that preferentially biases isotopic composition of any of the three groups analysed – Megateuthididae, Passaloteuthididae, or brachiopods, despite differences in Mg/Ca and Sr/Ca between these groups. We therefore convert from measured $\delta^{88/86}Sr_{cal}$ to the $\delta^{88/86}Sr_{sw}$ using the fractionation factor of 0.21 ‰ ($\Delta^{88/86}Sr_{sw}$ – carb), following Vollstaedt *et al.* (2014).

Temperature: in our samples, temperature does not correlate with $\delta^{88/86}Sr_{cal,}$ either overall or in any taxonomic group (Fig. 4a), so we do not correct for temperature dependency. Little temperature dependence has been reported for the calcitic foraminifera *G. ruber* (Böhm *et al.* 2012) or for modern calcitic terebratulid brachiopods (Vollstaedt *et al.* 2014). For the modern aragonitic coral *Pavona clavus*, Fietzke and Eisenhauer (2006) reported a dependence of +0.033 ‰ / °C.

Calcification rate: an inverse correlation between $\delta^{88/86}Sr_{cal}$ and Sr/Ca for biogenic calcite has been reported (Böhm *et al.* 2012) and appears also to extend to inorganic calcite (Al-Khatib and Eisenhauer 2017). The latter show that a single inverse correlation fits both inorganic calcite and biogenic calcite from a range of taxa. The inverse relation is ascribed to a kinetic control on the incorporation of Sr into the biogenic calcite structure (Stoll and Schrag, 2000, *et seq.*). In our samples $\delta^{88/86}Sr_{cal}$ is independent of Sr/Ca (Fig. 4b), so we make no correction for calcification rate.

4. Results and Discussion

4.1. Stratigraphic profile of $\delta^{44/40}Ca$

For presentation of the stratigraphic profile of $\delta^{44/40}Ca_{cal}$ (Fig. 5), we show base values in (a), temperature-corrected values in (b), and detrended-values in (c). In Table 1 are given the mean and 2s.e. values for $\delta^{44/40}Ca_{cal}$ in each of the three redox intervals shown in Fig. 2. Values of base-$\delta^{44/40}Ca_{cal}$ (Fig. 5a) decrease by around 0.05‰ through the Tenuicostatum Zone then, up-section, show a positive excursion of around 0.4 ‰ through the early part of the euxinic interval followed by decreasing values to the top of the section.

Temperature-corrected values (Fig. 5b) are around 1.50 ‰ at the base of the section, decrease to 1.45 ‰ at around 8 m before showing a small positive spike of around 0.25 ‰ at the beginning of the *exaratum* Subzone. Values then decrease up-section to around 1.45 ‰ at the top of the profile. The most positive 30% of the temperature-corrected $\delta^{44/40}Ca_{cal}$ of Brazier *et al.* (2015; also corrected to 15°C) agrees well with our temperature-corrected $\delta^{44/40}Ca_{cal}$.

Our interpretation remains robust when the assumption of uniform $\delta^{18}O_{sw}$ at both sample sites is abandoned. We modelled the effect of having different $\delta^{18}O_{sw}$ in Peniche and Yorkshire, and of having different $\delta^{18}O_{sw}$ in the euxinic interval in Yorkshire and outside it (Supplementary Information Figs. S3 and S4). We did so by varying the $\delta^{18}O_{sw}$ in Yorkshire whilst keeping it −1‰ in Peniche for an ice-cap-free world, and separately by varying the $\delta^{18}O_{sw}$ in the euxinic interval in Yorkshire whilst keeping $\delta^{18}O_{SW}$ outside it at −1‰. In both cases, we monitored the size of the small positive anomaly (Fig. 5) in the lower part of Interval 2 (Fig. 2). We also monitored the correlation coefficient (Fig. 3a) for the relation between temperature and $\delta^{44/40}Ca$. The detailed results of the sensitivity modelling are given in the Supplementary Information (Fig. S3) and summarised here.

Values of $\delta^{18}O_{sw}$ more positive than −1 ‰ in Yorkshire flatten the profile of temperature-corrected $\delta^{44/40}Ca$ seen in Fig. 5 and lessen (but do not remove) the small positive excursion in the lower part of Interval 2. The values, however, give implausibly high palaeo-temperatures of up to 45 °C in Yorkshire (Fig. S3). Values of $\delta^{18}O_{sw}$ in Yorkshire more negative than −1 ‰ increase the positive anomaly in the lower part of Interval 2, largely because both temperature, and so the temperature correction, are decreased (Fig. S3). Values more negative than −1 ‰ for $\delta^{18}O_{sw}$ also seriously degrade the correlation between temperature and $\delta^{44/40}Ca$; from 0.81 at −1 ‰ to 0.69 at −2 ‰ (Fig. S3). In short, no realistic variation across our sites in $\delta^{18}O_{sw}$ can generate negative excursions in $^{44}Ca/^{40}Ca$ through our composite section.

Values of detrended-$\delta^{44/40}Ca_{cal}$ (Fig. 5c) show a small decline of around 0.05 ‰ from the base of the section to around the 3 m level, above which the trend appears essentially unchanged to the top of the section. The key point is that, no matter what correction is applied, no negative excursion of $\delta^{44/40}Ca_{cal}$ can be generated in the interval between the mid *semicelatum I* and lower *exaratum* subzones (Interval 2 of Fig. 2), as would be expected were ocean acidification to have occurred.

4.2. Stratigraphic profile of $\delta^{88/86}Sr$

In Fig. 6 we show the profile of $\delta^{88/86}Sr_{sw}$ against stratigraphic level. Values increase from around 0.39 ‰ at the base of the section to 0.41 ‰ at 8 – 20 m, and then decrease towards 0.39 ‰. At the top of the section. These changes are half the reproducibility of our standards of ± 0.040 ‰ (2.s.d) and so may not be real. The data for the Yorkshire belemnites are indistinguishable from the trend defined by belemnites and brachiopods from Peniche. The key point of Fig. 6 is that the profile does not show a negative excursion of $\delta^{88/86}Sr_{sw}$ in Interval 2 (Fig. 2, mid *semicelatum* to early *exaratum* time) when the effects of ocean acidification have been postulated to operate. The means and 2s.e. of $\delta^{88/86}Sr_{sw}$ in Intervals 1, 2, and 3, respectively are given in Table 1.

4.3. Explaining the trends: $\delta^{44/40}Ca$

To assist interpretation of our trends, we first examine two other time-intervals for which negative excursions in $^{44}Ca/^{40}Ca$ have been demonstrated at times of LIP volcanism *viz.* the Permian – Triassic and the Cretaceous – Paleogene boundary intervals. We also compare our data to models of the observed profiles in a further attempt to constrain explanations of our data.

The Permian-Triassic boundary interval was a time of major extinction and LIP volcanism arising from emplacement of the Siberian Traps. The volcanism is widely credited with driving the extinctions and other environmental change. The boundary interval shows negative excursions in $\delta^{44/40}Ca$ of up to 0.6‰, the magnitude depending on location or where the baseline is placed before and after the excursion (Payne *et al.* 2010, Hinojosa *et al.* 2012, Silva-Tamayo *et al.* 2018, Wang *et al.* 2019). The excursion has been attributed to ocean acidification (Payne *et al.* 2010); "an imbalance between calcium weathering and burial fluxes triggered by ocean acidification" (Hinojosa *et al.* 2012); and a combination of initial ocean acidification (to generate the negative excursion) and a subsequent enhancement of silicate weathering, coupled to mineralogical change and, perhaps, the degree of saturation of seawater in carbonate, for the recovery (Silva-Tamayo *et al.* 2018). In contrast, Wang *et al.* (2019), noting that the P/T boundary was a time of major regression, invoke simple subaerial exposure and dissolution of shelf carbonates during that regression to explain negative isotope excursions in both $^{44}Ca/^{40}Ca$ and $^{88}Sr/^{86}Sr$ across the P/T interval: unless that dissolution was driven by acid waters resulting from LIP volcanism, the mechanism does not explain the C-isotope excursion across the P/T boundary.

The end-Cretaceous boundary interval was also a time of major extinction arising from CO_2 and SO_2 from both LIP volcanism (Deccan Traps) and the end-Cretaceous meteorite impact into Yucatan evaporites and carbonates. A negative excursion in $\delta^{44/40}Ca$ of 0.2 – 0.3 ‰ occurs across the Cretaceous – Palaeogene boundary, together with some variation before it (Linzmeier *et al.* 2019); the magnitudes of the excursions depend on where the baseline is placed.

For the Permo-Triassic interval, Silva-Tamayo et al. (2018) and Komar and Zeebe (2016) used coupled Ca- and C-modelling of $\delta^{44/40}Ca$ and $\delta^{13}C$ to simulate the effect on $\delta^{13}C$ and $\delta^{44/40}Ca$ in seawater. Neither model was able to explain how ocean acidification alone could generate the magnitude of the negative excursion in $\delta^{44/40}Ca$, so the models invoke mechanisms additional to volcanogenic-CO_2 to fully explain the C- and Ca-isotope excursions. In the case of the Cretaceous – Palaeogene boundary interval, modelling also failed to account for the magnitude of the Ca-isotope excursion, so biological fractionation (a vital effect) was invoked to explain the changes in $\delta^{44/40}Ca$ (Linzmeier *et al.* 2019). What modelling does not do is remove the reality of the excursions, or the fact that they occur at times of LIP volcanism, or the fact that, for the Permian – Triassic boundary interval, ocean acidification appears confirmed by $\delta^{11}B$-isotope profiles (Jurikova *et al.* 2020).

Models are indicative, not proscriptive, as Silva-Tamayo *et al.* (2018) acknowledge. The models noted above include numerous assumptions *e.g.* regarding the response of fractionation of Ca-isotopes to saturation state and carbonate-ion concentration in seawater (*cf.* Tang *et al.* 2008, Lemarchand *et al.* 2004, Al-Khatib and Eisenhauer 2017). Neither do models include the effects of injection into the atmosphere of SO_2 and HCl (Black *et al.* 2012; Schmidt *et al.* 2016, Jones et al. 2016), injections that would have enhanced acidification and added to CO_2 by titrating existing alkalinity. Nevertheless, models give a sense of direction for expected excursions, even if the magnitudes may be poorly calibrated, so we compare our measurements to qualitative representations of the models of Silva-Tamayo *et al.* (2018) that indicate what might be expected from ocean acidification and other scenarios of climate-change.

Outputs from the models of Silva-Tamayo *et al.* (2018) are shown in Fig. 7. The relevant model scenarios are: A, ocean acidification as a result of increased atmospheric CO_2 from LIP volcanism, B; an increase in alkalinity as a result of oceanic anoxia (more sulphate reduction); C an increase in weathering and so increased nutrient flux to the ocean, leading to increased flux of calcite and organic matter to the ocean floor and so increased burial of ^{12}C-enriched carbon and ^{40}Ca-enriched calcite.

Our profiles of $\delta^{44/40}Ca$ and $\delta^{13}C$ in Fig. 5 do not accord with any of the outputs shown in Fig. 7. Neither does combining the models in Fig. 7 lead to linear profiles that match those we report (Supplementary Information Fig. S5). A negative excursion in $\delta^{44/40}Ca_{cal}$ is not seen in our data in the upper *semicelatum* to mid-*exaratum* interval, whether the data is corrected or uncorrected (Fig. 5). The profile of temperature-corrected $\delta^{44/40}Ca_{cal}$ shows a barely-resolved positive excursion at the top of the *semicelatum 1* Subzone, which is the opposite of what is expected from ocean acidification. Furthermore, the detrended values of $\delta^{44/40}Ca_{cal}$ do not show any resolvable positive or negative excursion. These profiles allow us to reject the hypothesis that ocean acidification occurred in the *exaratum* Sz.

The absence of trends in our detrended-$\delta^{44/40}Ca$ profile cannot arise from chance compensation amongst the three forcings shown in Fig. 7; combining them (Fig. S5) modifies, but does not remove, the modelled stratigraphic variations *i.e.* does not yield the unvarying profile we document.

Ocean acidification might explain the minimum in temperature-corrected $\delta^{44/40}Ca_{cal}$ at around 8 m in the section (Fig. 5b) but the minimum is not seen in data detrended with Mg/Ca (Fig. 5c) nor is it seen in our profile of $\delta^{88/86}Sr_{cal}$ (Fig. 6). If real, it occurs below the putative acidification zone in Interval 2. The apparent minimum may be an artefact of the shortness of, and condensation in, the section: a longer section might show a background value of 1.45 ‰ superimposed on which are two positive excursions centred on 0 m and 12 m in the section – only a longer profile interval can resolve this issue. The shortness of the record is a problem that affects the interpretation of many Toarcian isotopic profiles. Without definition of a long-term trend that establishes a background trend (the baseline) for any variable (here, isotopic profiles through time), it is difficult to interpret changes in those profiles. We contend that the interval from mid *Semicelatum I* time through the lower *exaratum* Subzone (the supposed interval of acidification) does not show a negative excursion in either $\delta^{44/40}Ca_{cal}$ or $\delta^{88/86}Sr_{sw}$, but longer and more densely populated records would establish this point with greater confidence.

Whatever data set is accepted (base-, temperature-corrected, or detrended), no profile of $\delta^{44/40}Ca$, nor the profile of $\delta^{88/86}Sr_{sw}$, shows a negative excursion in mid *semicelatum I* to *exaratum* time, so the data do not support the presence of ocean acidification during this interval. Not making corrections for temperature or calcification rate leaves positive isotope excursions. These findings are in accordance with the data of Müller *et al.* (2020), who provide a profile of $\delta^{11}B$ in brachiopod calcite through the Peniche section. Their samples contain up to 4% Al, and the samples they analysed for $\delta^{11}B$ contain up to 1.2% Al, possibly in palygorskite, a Mg-rich clay (Fig. S8). The samples most affected are in the dysoxic interval. When $\delta^{11}B$ is corrected for the effects of contamination by clays (Fig. 8), the data show no definite trend to lower values in Interval 2. Since $\delta^{11}B$ is sensitive to the pH of seawater, the corrected data indicate that the pH of seawater did not change through the interval, suggesting ocean acidification did not occur.

Neither is ocean acidification needed to explain our profiles. Allowance must be made for condensation of strata in the boundary interval (Elmi 2006, 2007; McArthur *et al.* 2020), which accentuates the apparent rate of change of all chemical and isotopic profiles in the lowermost 3m of the Toarcian section at Peniche: in Yorkshire, the *exaratum* Subzone is also condensed relative to underlying and overlying strata (McArthur *et al.* 2000). When allowance is made for condensation at Peniche, values of $\delta^{44/40}Ca_{cal}$ show no more variation per Ma through the interval of study, a period of between 1 and 3 myrs, than is seen through much of Phanerozoic time (de la Rocha and DePaolo 2000; Farkaš *et al.* 2007a,b).

Wider Considerations

Whilst it is not appropriate here to review the entirety of early Toarcian events in the light of our findings, a few merit attention. The first is the suggestion that ocean acidification led to the demise of carbonate platforms (Trecalli *et al.* 2012; Ettinger *et al.* 2021). That suggestion is not supported by our data. Furthermore, as Krencker *et al.* (2020) highlight, many other possible causes exist for platform demise, including a rise in sea-level, an event widely accepted as characterising the early Toarcian (Hallam 1988, 1997; Thibault *et al.* 2018).

The second worth mentioning is the weathering proxy based on osmium isotopes. Values of $^{187}Os/^{188}Os_{initial}$ in sediments below the *exaratum* Sz. are around 0.2 – 0.4 (Cohen *et al.* 2004, Porter *et al.* 2013; Percival *et al.* 2016; summary in Kemp *et al.* 2020) whilst above it values are around 0.4 (*ibid*). Yet values within the *exaratum* Sz. range from 0.4 to 1.0 (ibid). The high values of 0.8 to 1.0 in this subzone in Yorkshire, UK, were attributed by Cohen *et al.* (2004), and later, others, to enhanced weathering of continental crust. The low values of ≈ 0.4 in the *exaratum* Sz. in Dotternhausen, Germany, were attributed by van Acken *et al.* (2019) to weathering of LIP flood basalts. Such a large range in $^{187}Os/^{188}Os_{initial}$ values in the *exaratum* Sz., and such conflicting interpretations, pose problems for the use of Os isotopes as a global weathering proxy, at least for this interval. The large differences in values of $^{187}Os/^{188}Os_{initial}$ between sites for the same time period might be better explained in other ways. Those ways include the operation of local effects, such as basin restriction and drawdown of Os, which sensitizes isolated basins to riverine inputs and magnifies crustal contributions from waters above a pycnocline (McArthur *et al.* 2008; McArthur

2019); such an influence probably provides the best explanation for the large variations in the Mo-isotope composition of sediments across northern Tethys (compare Pearce *et al.* 2008 with Dickson *et al.* 2017).

Finally, the early Toarcian trends in $\delta^{13}C$ are usually described as broad positive excursions (in both organic matter and carbonate) on which, in Interval 2, are superimposed negative excursions in $\delta^{13}C_{org}$ and $\delta^{13}C_{cal}$, both being driven either by volcanogenic CO_2 (Karoo-Ferrar), or the release of methane from clathrates (*e.g.* Hesselbo *et al.* 2000, Ruebsam *et al.* 2020). Such release would drive ocean acidification. Others point to difficulties with these suggested drivers of Toarcian trends in $\delta^{13}C$. Notably, van de Schootbugge *et al.* (2005) highlighted the large range from place-to-place in the magnitude of the putative negative changes in $\delta^{13}C$ in the *exaratum* Sz. Such variation is usually explained as 'local' effects moderating a 'global' signal but, other than basin restriction, the mechanisms driving those local effects are not explained.

For inorganic carbon, no global component needed if one views the trends in $\delta^{13}C_{cal}$ through the Pliensbachian and Toarcian as simply comprising three separate positive excursions (two in the Toarcian) with a return to background between each (*c.f.* McArthur 2007). Such a view seems the best explanation for isotopic profiles that cover a period long enough to define background values below and above both positive excursions *e.g.* the Trento Platform (see Fig. 3 of Ettinger *et al.* 2021, reproduced here as Fig. S14) and the Nianduo Section, Tibet (see Fig. 3 of Han *et al.* 2018).

For organic carbon, van de Schootbrugge *et al.* (2013) and Suan *et al.* (2015) showed that variations in $\delta^{13}C_{org}$ cannot be interpreted correctly in the absence of accompanying analysis for hydrogen index (HI). Correcting $\delta^{13}C_{org}$ for variations in HI substantially reduces variations in $\delta^{13}C_{org}$ (*bid.*) and can remove entirely some negative excursions seen in uncorrected data (Schöllhorn *et al.* 2019). After correcting for variation in HI, van de Schootbrugge *et al.* (2013) and Suan *et al.* (2015) explained a residual apparent isotopic change of −3‰ in the *exaratum* Sz. of NW Europe as arising from a contribution to sediment organic-matter of bacterial biomass originating in the redoxcline of a redox-stratified water-mass. These authors thus revitalise the Küspert model for the interval (Küspert 1982; Saelen *et al.* 1989) as an explanation for trends in $\delta^{13}C_{org}$ in the *exaratum* Sz. Our failure to detect ocean acidification in that subzone further informs this debate.

6. Conclusions

No negative excursion was found in $\delta^{44/40}Ca$ of biogenic calcite, or of $\delta^{88/86}Sr_{sw}$, through the interval from the mid *semicelatum* Subzone to the end *exaratum* Subzone, an interval commonly termed an oceanic anoxic event. It follows that ocean acidification postulated for the interval was insufficient to disturb oceanic $^{44}Ca/^{40}Ca$ or $^{88}Sr/^{86}Sr$ enough for our analysis to detect its effect, in contrast to other intervals of time when boundary excursions in $\delta^{44/40}$Ca occurred and have been attributed to ocean acidification (*e.g.* Payne *et al.* 2010; Jost *et al.* 2017, Silva-Tamayo et al. 2018).

Values of $\delta^{44/40}$Ca in Passaloteuthididae belemnites, Megateuthididae belemnites, and brachiopods of the species *Soaresirhynchia bouchardi*, show a positive correlation between $\delta^{44/40}$Ca and temperature with a temperature sensitivity of +0.020 ± 0.004 ‰/°C (2.s.d.). For belemnites only, $\delta^{44/40}$Ca correlates positively with Mg/Ca and Sr/Ca. Values of $\delta^{88/86}Sr_{cal}$ are independent of temperature and Sr/Ca.

Acknowledgements

We thank 3 anonymous reviewers for comments that were perceptive and constructive, and L.V. Duarte for assistance in the field.

Statement of Funding. This work was funded by grant RPG-2014-399 from the Leverhulme Trust.

References:

Al-Khatib M. and Eisenhower A. 2017. Calcium and strontium isotope fractionation in aqueous solutions as a function of temperature and reaction rate; I. Calcite. *Geochim. Cosmochim. Acta*, **209**, 296–319.

~~Al-Suwaidi A.H., Angelozzi G.N., Baudin F., Damborenea SE. Hesselbo S.P., Jenkyns H.C., Manceñido M.O., Riccardi A.C. 2010. First record of the Early Toarcian Oceanic Anoxic Event from the Southern Hemisphere, Neuquen Basin, Argentina. *Jour. Geol. Soc. London*, **167(4)**, 633–636~~

Bailey T.R., Rosenthal Y., McArthur J.M., van de Schootbrugge B. and Thirlwall M.F. 2003. Paleoceanographic changes of the Late Pliensbachian–Early Toarcian interval: a possible link to the genesis of an Oceanic Anoxic Event. *Earth Planet. Sci. Letters*, **212**, 307–320.

Bajnai D., Guo W., Spötl C., Coplen T.B., Methner K., Löffler N., Krsnik E., Gischler E., Hansen M., Henkel D., Price G.D., Raddatz J., Scholz D., and Fiebig J. 2020. Dual clumped isotope thermometry resolves kinetic biases in carbonate formation temperatures. Nature Communications, 11234567890, doi.org/10.1038/s41467-020-17501-0.

Black B.A., Elkins-Tanton L.T., Rowe M.C. and Peate I.U. 2012. Magnitude and consequences of volatile release from the Siberian Traps. *Earth Planet. Sci. Letters,* **317–318**, 363–373.

Bradbury H. J. and Turchyn A. V. 2018. Calcium isotope fractionation in sedimentary pore fluids from ODP Leg 175: Resolving carbonate recrystallization. *Geochim.Cosmochim. Acta,* **236**, 121–139.

Brazier J-M., Suan G., Tacail T., Simon L., Martin J.E., Mattioli E and Balter V. 2015. Calcium isotope evidence for dramatic increase of continental weathering during the Toarcian oceanic anoxic event (Early Jurassic). *Earth and Planetary Science Letters* **411**, 164–176.

Bodin S., Mattioli E., Fröhlich S., Marshall J.D., Boutib L., Lahsini S. and Redfern J. 2010. Toarcian carbon isotope shifts and nutrient changes from the Northern margin of Gondwana (High Atlas, Morocco, Jurassic): palaeoenvironmental implications. *Palaeogeography, Palaeoclimatology, Palaeoecology*, **297**, 377–390.

Bodin S., Krencker F.-N., Kothe T., Hoffmann R., Mattioli E., Heimhofer U. and Kabiri L. 2016. Perturbation of the carbon cycle during the late Pliensbachian - Early Toarcian: New insight from high-resolution carbon isotope records in Morocco. *Journal of African Earth Sciences*, **116**, 89–104.

Böhm F., Eisenhauer A., Tang J., Dietzel M., Krabbenhöft A., Kisakürek B. and Horn C., 2012. Strontium isotope fractionation of planktic foraminifera and inorganic calcite. *Geochim. Cosmochim Acta*, **93**, 300–314.

Burgess S.D., Bowring S.A., Fleming T.H. and Elliot D.H. 2015. High-precision geochronology links the Ferrar large igneous province with early-Jurassic ocean anoxia and biotic crisis. *Earth Planet. Sci. Letters*, **415**, 90–99.

Caswell B.A., Coe A.L. and Cohen A.S. 2009. New range data for marine invertebrate species across the early Toarcian (Early Jurassic) mass extinction. *Jour. Geol. Soc. London*, **166**, 859–872. doi: 10.1144/0016-76492008-0831.

Caswell B.A. and Coe A.L. 2013. Primary productivity controls on opportunistic bivalves during Early Jurassic oceanic deoxygenation. *Geology*, **41(11)**, 1163–1166.

Cohen A.S., Coe A.L., Harding S.M. and Schwark L. 2004. Osmium isotope evidence for the regulation of atmospheric CO_2 by continental weathering. Geology, **32(2**), 157–160.

Daëron M., Drysdale R.N., Peral M., Huyghe D., Blamart D., Coplen T.B., Lartaud F. and Zanchett, G. 2019. Most Earth-surface calcites precipitate out of isotopic equilibrium. *Nature Communications*, **10:429**, doi.org/10.1038/s41467-019-08336-

Danise S., Twitchett R.J., Little C.T.S. and Clémence M-E. (2013). The impact of global warming and anoxia on marine benthic community dynamics: an example from the Toarcian (Early Jurassic). *PloS One*, **8(2)**, e56255.

De La Rocha C.L. and DePaolo D.J. 2000. Isotopic evidence for variations in the marine calcium cycle over the Cenozoic. *Science*, **289**, 1176–1178.

Dera G., Neige P., Dommergues J.-L., Fara E., Laffont R. and Pellenard P. 2010. High-resolution dynamics of Early-Jurassic marine extinctions: the case of Pliensbachian-Toarcian ammonites (Cephalopoda). *Jour. Geol. Soc. London*, **167**, 21–33.

de Villiers S., Greaves M. and Elderfield H. 2002. An intensity ratio calibration method for the accurate determination of Mg/Ca and Sr/Ca of marine carbonates by ICP-AES. *Geochem. Geophys. Geosyst.*, **3**, 10.1029/2001GC000169.

DePaolo D.J. 2011. Surface kinetic model for isotopic and trace element fractionation during precipitation of calcite from aqueous solutions. *Geochimica et Cosmochimica Acta*, **75(4)**, 1039–1056.

Dera G., Pellenard P., Neige P., Deconinck J-F., Pucéat E. and Dommergues J-L. 2009. Distribution of clay minerals in early Jurassic Peritethyan seas: palaeoclimatic significance inferred from multiproxy comparisons. *Palaeogeogr. Palaeoclimatol. Palaeoecol.*, **271(1–2)**, 39–51.

Dickson A.J., Gill B.C., Ruhl M., Jenkyns H.C., Porcelli D., Idiz E., Lyons T.W., van den Boorn S.H.J.M. 2017. Molybdenum-isotope chemostratigraphy and paleoceanography of the Toarcian Oceanic Anoxic Event (Early Jurassic). Paleoceanography, **32(8)**, 813–829.

Duarte L.V., Silva R.L., Félix F., Comas-Rengifo M.J., Rocha R.B., Mattioli E., Paredes R., Filho J.G.M. and Cabral M.C. (2017). The Jurassic of the Peniche Peninsula (Portugal): scientific, educational and science popularization relevance (El Jurásico de la Península de Peniche (Portugal): relevancia científica, educativa y divulgativa). *Revista de la Sociedad Geológica de España*, **30(1)**, 55–70.

Duarte L.V, Comas-Rengifo M.J., Hesselbo S., Mattioli E., Suan G., (coordinators), Baker S., Cabral M.C., Correia V., García Joral F., Goy A., Reolid M., Rita P., Félix F., Paredes R., Pittet B. and Rocha R.B. 2018. The Toarcian Oceanic Anoxic Event at Peniche. An exercise in integrated stratigraphy - Stop 1.3. *In*: Duarte L.V. and Silva R. (Eds). Field Trip Guidebook: The TOAE in the Western Iberian Margin and its context within the Lower Jurassic evolution of the Lusitanian Basin. Second International Workshop on Toarcian Oceanic Anoxic Event, Coimbra,, Portugal, 2018.

Elmi S. 2006. Pliensbachian/Toarcian boundary: the proposed GSSP of Peniche (Portugal). *Volumina Jurassica*, **4**, 5–16.

Elmi S. 2007. Pliensbachian/Toarcian boundary: the proposed GSSP of Peniche (Portugal). *Ciências da Terra/Earth Sciences Journal*, **16,** 7–16.

Ettinger N.P., Larson T.E., Kerans C., Thibodeau A.M., Hattori K.E., Kacur S.M. and Martindale R.C. 2021. Ocean acidification and photic-zone anoxia at the Toarcian Oceanic Anoxic Event: insights from the Adriatic carbonate platform. *Sedimentology*, **68**, 63–107.

Fantasia A., Adatte T., Spangenberg J.E., Font E., Duarte L.V. and Föllmi K.B. 2019. Global versus local processes during the Pliensbachian–Toarcian transition at the Peniche GSSP, Portugal: A multi-proxy record. Earth-Science Reviews, **198**, 102932.

Farkaš, J., Florian Böhm, Wallmann K., Blenkinsop J., Eisenhauer A., van Geldern R., Munnecke A., Voigt S., and Veizer J. 2007a. Calcium isotope record of Phanerozoic oceans: Implications for chemical evolution of seawater and its causative mechanisms. *Geochim.Cosmochim. Acta,* **71(21)**, 5117–5134.

Farkaš J., Buhl D., Blenkinsop J. and Veizer J. 2007b. Evolution of the oceanic calcium cycle during the late Mesozoic: Evidence from $\delta^{44/40}$Ca of marine skeletal carbonates. *Earth Planet. Sci. Letters,* **253(1)**, 96–111.

Fietzke J. and Eisenhauer A. 2006. Determination of temperature-dependent stable strontium isotope (^{88}Sr/^{86}Sr) fractionation via bracketing standard MC-ICP-MS. *Geochem. Geophys. Geosyst.*, **7**, Q08009, doi:10.1029/2006GC001243

French K.L., Sepúlveda J., Trabucho-Alexandre J., Gröcke D.R. and Summons R.E. 2014. Organic geochemistry of the earlyToarcian oceanic anoxic event in Hawsker Bottoms, Yorkshire, England. *Earth and Planetary Science Letters*, **390**, 116–127.

Gradstein F.M., Ogg J.G., Schmitz M.D. and Ogg G.M. (Eds) 2020. A Geologic Time Scale 2020. Elsevier, 2 Vols, 1357 pp.

Griffith E.M. Fantle M.S., Eisenhauer A., Paytan A. and Bullen T.D. 2015. Effects of ocean acidification on the marine calcium isotope record at the Paleocene–Eocene Thermal Maximum. *Earth Planet. Sci. Letters*, 419, 81–92.

Gussone N., Böhm F., Eisenhauer A., Dietzel M., Heuser A., Teichert B.M.A., Reitner J., Wörheide G., and Dullo W.-C. 2005. Calcium isotope fractionation in calcite and aragonite. *Geochimica et Cosmochimica Acta*, **69(18)**, 4485–4494.

Gussone N. and Heuser A. 2016. Biominerals and biomaterial. In: Gussone N., Schmitt A.-D., Heuser A., Wombacher F., Dietzel M., Tipper E. and Schiller M. (Eds.), Calcium Stable Isotope Geochemistry. Springer Heidelberg (260pp).

Hallam A. 1986. The Pliensbachian and Tithonian extinction events. *Nature*, **31**9, 765–768.

Hallam A. 1988. A re-evaluation of Jurassic eustasy in the light of new data and the revised Exxon curve. *In*: Wilgus, C.K. (Ed.), Sea-level Changes: An Integrated aAproach. Society of Economic Paleontologists and Mineralogists. Special Publications 42. pp. 261–273.

Hallam A. 1997. Estimates of the amount and rate of sea-level change across the Rhaetian-Hettangian and Pliensbachian-Toarcian boundaries (latest Triassic to Early Jurassic). *J. Geol. Soc. Lond.* **154**, 773–779.

Han Z., Hu X., Kemp D.B. and Li J. 2018. Carbonate-platform response to the Toarcian Oceanic Anoxic Event in the southern hemisphere: implications for climatic change and biotic platform demise. *Earth Planet. Sci. Lett.*, **489**, 59–71

Harries P.J. and Little C.T. 1999. The early Toarcian (Early Jurassic) and the Cenomanian–Turonian (Late Cretaceous) mass extinctions: similarities and contrasts. *Palaeogeography, Palaeoclimatology, Palaeoecology*, **154**, 39–66.

Hays P.D. and Grossman E.L. 1991. Oxygen isotopes in meteoritic calcite cements as indicators of continental paleoclimate. *Geology*, **19(5)**, 441–444.

Harazim D., van de Schootbrugge B., Sorichter K, Fiebig J., WeugA., Suan G., Oschmann W. 2013. Spatial variability of watermass conditions within the European Epicontinental Seaway during the Early Jurassic (Pliensbachian–Toarcian). *Sedimentology*, **60**, 359–390.

Hermoso M., Minoletti F. Le Callonnec L., Jenkyns H.C., Hesselbo S.P., Rickaby R.E.M., Renard, M., Rafélis M. and Emmanuel L. 2009. Global and local forcing of Early Toarcian seawater chemistry: a comparative study of different paleoceanographic settings (Paris and Lusitanian basins). *Paleoceanography*, **24**, PA4208, doi:10.1029/2009PA001764.

Hesselbo S.P., Gröcke, D.R., Jenkyns, H.C., Bjerrum, C.J., Farrimond, P., Morgans Bell, H.S. and Green, O.R. 2000. Massive dissociation of gas hydrate during a Jurassic oceanic anoxic event, *Nature*, **406**, 392–395.

Hesselbo S.P., Jenkyns H.C., Duarte L.V. and Oliveira L.C.V. 2007. Carbon-isotope record of the Early Jurassic (Toarcian) Oceanic Anoxic Event from fossil wood and marine carbonate (Lusitanian Basin, Portugal). *Earth Planet. Sci. Letters*, **253**, 455–470.

Hinojosa J.L., Brown S.T., Chen J., DePaolo D.J. Paytan A., Shen S-Z., and Payne J.L. 2012. Evidence for end-Permian ocean acidification from calcium isotopes in biogenic apatite. Geology, **40(8)**, 743–746.

Howarth M.K. 1962. The Jet Rock series and the Alum Shale series of the Yorkshire coast. *Proceedings of the Yorkshire Geological Society*, **33(4)**, 381–422.

Howarth M.K. 1991–1992. The ammonite family Hildoceratidae in the Lower Jurassic of Britain. *Monographs of the Palaeontographical Society*, London: 200pp, 38pl.

Ivanov A.V., Meffre S., Thompson J., Corfu F., Kamenetsky V.S., Kamenetsky M.B. and Demonterova, E.I. 2017. Timing and genesis of the Karoo-Ferrar large igneous province: new high precision U-Pb data for Tasmania confirm short duration of the major magmatic pulse. *Chemical Geology*, **455**, 32–43.

Jenkyns H. 1988. The Early Toarcian (Jurassic) anoxic event: stratigraphic, sedimentary and geochemical evidence. *Am. Jour. Sci.* 288, 101–151.

Jones M.T., Jerram D.A., Svensen H.H. and Grove C., 2016. The effects of large igneous provinces on the global carbon and sulphur cycles. Palaeogeography, Palaeoclimatology, Palaeoecology, **441**, 4–-21.

Jost A.B., Bachan A., van de Schootbrugge B., Brown S.T., DePaolo D.J. and Payne J.L. 2017. Additive effects of acidification and mineralogy on calcium isotopes in Triassic/Jurassic boundary limestones. *Geochemistry, Geophysics, Geosystems*, **18(1)**, 113–124.

Jourdan, F., Féraud, G., Hervé, B., Kampunzu, A.B., Tshoso, G., Watkeys, M.K. and Gall, B.L. 2005. Karoo large igneous province: Brevity, origin, and relation to mass extinction questioned by new ^{40}Ar/^{39}Ar age data. *Geology*, **33(9)**, 745–748.

Jourdan F., Féraud G., Bertrand H. and Watkeys M.K. 2007. From flood basalts to the inception of oceanization: example from the 40Ar/39Ar high-resolution picture of the Karoo large igneous province. *Geochem. Geophysics Geosystems*, **8(2)**, Q02002, doi:10.1029/2006GC001392

Jourdan F., Féraud G., Bertrand H., Watkeys M.K. and Renne P.R. 2008. The ^{40}Ar/^{39}Ar ages of the sill complex of the Karoo large igneous province: implications for the Pliensbachian- Toarcian climate change. *Geochemistry, Geophysics, Geosystems*, **9(6)**, Q06009.

Jurikova H., Gutjahr M., Wallmann K., Flögel S., Liebetrau V., Posenato R., Angiolini L., Garbelli C., Brand U., and Wiedenbeck M. and Eisenhauer A. 2020. Permian–Triassic mass extinction pulses driven by major marine carbon cycle perturbations. *Nature Geoscience*, 13, 745–750.

Kemp D.B., Coe A.L., Cohen A.S., Schwark L. 2005. Astronomical pacing of methane release in the Early Jurassic period. *Nature*, **437**, doi:10.1038/nature04037.

Kemp D.B. and Izumi K. 2014. Multiproxy geochemical analysis of a Panthalassic margin record of the early Toarcian oceanic anoxic event (Toyora area, Japan). Palaeogeog. Palaeoclimatol, Palaeoecol, 414, 332–341.

Kemp D.B., Selby D., and Izumi K., 2020. Direct coupling between carbon release and weathering during the Toarcian oceanic anoxic event. Geology, 48, 976–980.

Kisakürek B., Eisenhauer A., Böhm F., Hathorne E.C. and Erez J. 2011. Controls on calcium isotope fractionation in cultured planktic foraminifera, *Globigerinoides ruber* and *Globigerinella siphonifera*. *Geochim. Cosmochim. Acta*, **75**, 427–443.

Komar N. and Zeebe R.E. 2016. Calcium and calcium isotope changes during carbon cycle perturbations at the end-Permian. *Paleoceanography*, **31**, 115–130.

Krabbenhöft A., Fietzke J., Eisenhauer A., Liebetrau V., Böhm F. and Vollstaedt H. 2009. Determination of radiogenic and stable strontium isotope ratios (^{87}Sr/^{86}Sr; δ^{88}/^{86}Sr) by thermal ionization mass spectrometry applying an ^{87}Sr/^{84}Sr double spike. *Journal of Analytical Atomic Spectrometry*, **24(9)**, 1267–1271.

Krencker F.-N., Fantasia A., Danisch J., Martindale R., Kabiri L., El Ouali M. and Bodin S. 2020. Two-phased collapse of the shallow-water carbonate factory during the late Pliensbachian-Toarcian driven by changing climate and enhanced continental weathering in the Northwestern Gondwana Margin. *Earth-Science Reviews*, **208**, 103254.

Küspert W. 1982. Environmental changes during oil shale deposition as deduced from stable isotope ratios. In *Cyclic and event stratification* (pp. 482–501). Springer, Berlin, Heidelberg.

Lemarchand, D., Wasserburg, G.J. and Papanastassiou, D.A., 2004. Rate-controlled calcium isotope fractionation in synthetic calcite. Geochimica et Cosmochimica Acta, **68(22)**, pp.4665-4678.

Li Q., Thirlwall M. and Müller W. 2016. Ca isotopic analysis of laser-cut microsamples of (bio) apatite without chemical purification. *Chem. Geol.* **422**, 1–12.

Linzmeier B.J., Jacobson A.D., Sageman B.B., Hurtgen M.T., Ankney M.E., Petersen S.V., Tobin T.S., Kitch G.D., and Wang J. 2019. Calcium isotope evidence for environmental variability before and across the Cretaceous-Paleogene mass extinction. Geology, **48**, 34–38.

Little C.T.S. and Benton M.J. 1995. Early Jurassic mass extinction: a global long-term event. *Geology*, **23(6)**, 495–498.

Mattioli, E., Pittet, B., Petitpierre, L., Mailliot, S., 2009. Dramatic decrease of pelagic carbonate production by nannoplankton across the Early Toarcian anoxic event (TOAE). Global Planet. Change, **65(3/4)**, 134–145.

McArthur J.M., Donovan D.T., Thirlwall M.F., Fouke B.W. and Mattey D. 2000. Strontium isotope profile of the early Toarcian (Jurassic) oceanic anoxic event, the duration of ammonite biozones, and belemnite palaeotemperatures. *Earth Planet. Sci. Letters*, **179**, 269–285.

McArthur J.M. 2007. Comment on “Carbon-isotope record of the Early Jurassic (Toarcian) Oceanic Anoxic Event from fossil wood and marine carbonate (Lusitanian Basin, Portugal)” by Hesselbo S., Jenkyns H.C., Duarte L.V. and Oliveira L.C.V. *Earth and Planetary Science Letters* **259**, 634–639.

McArthur J.M., Algeo T.J., Van de Schootbrugge B., Li Q. and Howarth R.J. 2008. Basinal restriction, black shales, Re- Os dating, and the Early Toarcian (Jurassic) oceanic anoxic event. *Paleoceanography*, **23(4)**. PA4217, doi:10.1029/2008PA001607.

McArthur J.M. 2019. Early Toarcian black shales: a response to an oceanic anoxic event or anoxia. in marginal basins? *Chem. Geol.*, **522**, 71–83.

McArthur J.M., Page K, Duarte L.V., Thirlwall M.F., Li Q. and Weis R. 2020. Sr-isotope stratigraphy ($^{87}Sr/^{86}Sr$) of the lowermost Toarcian of Peniche, Portugal, and its relation to ammonite zonations. *Newsletters on Stratigrphy*, 53(3), 297–312. DOI: 10.1127/nos/2019/0492.

McConnaughey T. 1989. ^{13}C and $^{18}0$ isotopic disequilibrium in biological carbonates: I. Patterns *Geochim. Cosmochim. Acta*, **53**, 151–162.

Moulin M., Fluteau F., Courtillot V., Marsh J., Delpech G., Quidelleur X. and Gérard M. 2017. Eruptive history of the Karoo lava flows and their impact on early Jurassic environmental change. *J. Geophys. Res. Solid Earth*, **122**, 738–772.

Mouterde R. 1955. Le Lias de Peniche. Direcção general de minas e Serviçios geológicos.

Mouterde R. 1967. Le Lias du Portugal: vue d'ensemble et division en zones. *Comun. Serv. Geol. Portugal*, **52**, 209–226.

Müller T., Jurikova H., Gutjahr M., Tomašových A., Schlög J., Liebetrau V., Duarte L.V., Milovský R., Suan G., Mattioli E., Pittet B and Anton Eisenhauer. 2020. Ocean acidification during the early Toarcian extinction event: evidence from boron isotopes in brachiopods. *Geology*, **48**, https://doi.org/10.1130/G47781.1.

Nägler T.F., Eisenhauer A., Müller A., Hemleben C. and Kramers J. 2000. The $\delta^{44}Ca$-temperature calibration on fossil and cultured *Globigerinoides sacculifer*: new tool for reconstruction of past sea-surface temperatures. *Geochem. Geophys. Geosyst.*, **1**, 2000GC0000091.

Nielsen L.C., Druhan J.L., Yang W., Brown S.T. and DePaolo D.J. 2012. Calcium Isotopes as Tracers of Biogeochemical Processes. *In*: Baskaran M. (eds) Handbook of Environmental Isotope Geochemistry. Advances in Isotope Geochemistry. Springer, Berlin, Heidelberg.

Page K.N. 2004. A sequence of biohorizons for the Subboreal Province Lower Toarcian in Northern Britain and their correlation with a Submediterranean Standard. *Rivista Italiana di Paleontologia e Stratigrafia*, **110**, 109–114.

Pálfy J. and Smith P.L. 2000. Synchronony between Early Jurassic extinction, oceanic anoxic event, and the Karoo–Ferrar flood basalt volcanism. *Geology*, **28**, 747–750.

Payne J.L., Turchyn A.V., Paytan A., DePaolo D.J., Lehrmann D.J., Yu M. and Wei J. 2010. Calcium isotope constraints on the end-Permian mass extinction. *Proceedings of the National Academy of Sciences*, **107(19)**, 8543–8548.

Pearce C.R., Cohen A.S., Coe A.L., Burton K.W. 2008. Molybdenum isotope evidence for global oceanic anoxia coupled with perturbations to the carbon cycle during the Early Jurassic. *Geology*, **36**, 231–234.

Penman, D. E., Hönisch B., Zeebe R.E., Thomas E. and Zachos J.C. 2014. Rapid and sustained surface ocean acidification during the Paleocene-Eocene Thermal Maximum, *Paleoceanography*, 29, 357–369, doi:10.1002/2014PA002621.

Percival L.M.E., Cohen A.S., Davies M.K., Dickson A.J., Hesselbo S.P., Jenkyns H.C., Leng M.J.,

Mather T.A. 2016. Osmium isotope evidence for two pulses of increased continental weathering linked to Early Jurassic volcanism and climate change. *Geology*, **44(9)**, 759–762.
Pittet B., Suan G., Lenoir F., Duarte L.V., and Mattioli L.V. 2014. Carbon isotope evidence for sedimentary discontinuities in the lower Toarcian of the Lusitanian Basin (Portugal): Sea level change at the onset of the Oceanic Anoxic Event. *Sed. Geol.*, **303**, 1–14.
Porter S.J., Selby D., Suzuki K. and Gröcke D. 2013. Opening of a trans-Pangaean marine corridor during the Early Jurassic: insights from osmium isotopes across the Sinemurian–Pliensbachian GSSP, Robin Hood's Bay, UK. Palaeogeog. Palaeoclimatol. Palaeoecol., **375,** 50–58.

Raup D.M. and Sepkowsi J.J. Jr. 1986. Periodic extinction of families and genera. *Science*, **231**, 833–836.
Reynard L.M., Henderson G.M. and Hedges R.E.M. 2010. Calcium isotope ratios in animal and human bone. *Geochim. Cosmochim. Acta*, **74(13)**, 3735–3750.
Rocha R. B., Mattioli E., Duarte L. V., Pittet B., Elmi S., Mouterde R., Cabral M.-C., Comas-Rengifo M.-J., Gómez J.J., Goy A., Hesselbo S.P., Jenkyns H.C., Littler K., Mailliot S., Luiz Oliveira L., C., Veiga, Osete M.-L., Perilli N., Pinto S., Ruget C. and Suan G. 2016. Base of the Toarcian Stage of the Lower Jurassic defined by the Global Boundary Stratotype Section and Point (GSSP) at the Peniche section (Portugal). *Episodes*, **39(3)**, 460–481.
Röhl H.-J., Schmid-Röhl A., Oschmann W., Frimmel A., Schwark L. 2001. The Posidonia Shale (lower Toarcian) of SW Germany: an oxygen depleted ecosystem controlled by sealevel and palaeoclimate. *Palaeogeogr. Palaeoclimatol. Palaeoecol.* **169**, 273–299.
Rosales I., Quesada S. and Robles S. 2004. Paleotemperature variations of Early Jurassic seawater recorded in geochemical trends of belemnites from the Basque-Cantabrian basin, northern Spain. *Palaeogeog. Palaeoclimatol. Palaeoecol.*, **203**, 253–275.
Ruebsam W., Mayer B.and Schwark L. 2019. Cryosphere carbon dynamics control early Toarcian global warming and sea level evolution. *Global and Planetary Chenge*, **172**, 440–453.
Sælen G., Doyle P. and Talbot M.R. 1996. Stable isotope analyses of belemnite rostra from the Whitby Mudstone Fm., England: surface water conditions during deposition of a marine black shale. *Palaios*, 11, 97–117.
Schmidt A., Skeffington R.A., Thordarson T., Self S., Forster P.M., Rap A., Ridgwell A., Fowler D., Wilson M., Mann G.W., Wignall P.B. and Carslaw K.S. 2016. Selective environmental stress from sulphur emitted by continental flood basalt eruptions. *Nature Geoscience*, **9**, 77–82.
Schmid-Röhl A., Röhl H., Oschmann J.W., Frimmel A., Schwark L., 2002. Palaeoenvironmental reconstruction of Lower Toarcian epicontinental black shales (Posidonia shale, SW Germany): global versus regional control. *Geobios*, **35**, 13–20.
Schouten S., Van Kaam-Peters H.M.E., Rijpstra W.I.C., Schoell M., Sinninghe Damsté J.S., 2000. Effects of an oceanic anoxic event on the stable carbon isotopic composition of Early Toarcian carbon. *Am. J. Sci.* **300**, 1–22.
Schöllhorn I., Adatte T., Van de Schootbrugge B., Houben A., Charbonnier G., Janssen N., Föllmi K.B. 2020. Climate and environmental response to the break-up of Pangea during the Early Jurassic (Hettangian-Pliensbachian); the Dorset coast (UK) revisited. *Global and Planetary Change*, **185**, 103096.
Silva-Tamayo J.C., Lau K.V., Jost A.B., Payne J.L., Wignall P.B., Newton R.J., Eisenhauer A., Depaolo D.J., Brown S., Mahe, K. and Lehrmann D.J., 2018. Global perturbation of the marine calcium cycle during the Permian-Triassic transition. *Bulletin*, **130(7–8)**, 1323–1338.
Skulan J., DePaolo D.J. and Owens T. 1997. Biological control of calcium isotopic abundances in

the global calcium cycle. *Geochim. Cosmochim. Acta*, **61**, 2505–2510.

Stoll H. M. and Schrag D. P. 2000. Coccolith Sr/Ca as a new indicator of coccolithophorid calcification and growth rate. *Geochem., Geophys., Geosystems*., **1**, 1–24.

Suan G., Mattioli E, Pittet B., Mailliot S. and Lécuyer C. 2008. Evidence for major environmental perturbation prior to and during the Toarcian (Early Jurassic) oceanic anoxic event from the Lusitanian Basin, Portugal. *Paleoceanography*, PA1202, doi:10.1029/2007PA001459, 14 pp.

Suan G., Mattioli E., Pittet B., Lécuyer C., Suchéras-Marx B., Duarte L.V., Philippe M., Reggiani L. and Martineau F. 2010. Secular environmental precursors to Early Toarcian (Jurassic) extreme climate changes. *Earth Planet. Sci. Letters*, **290**, 448–458.

Suan G., van de Schootbrugge B., Adatte T., Fiebig J. and Oschmann W. 2015. Calibrating the magnitude of the Toarcian carbon cycle perturbation. Paleoceanography, **30**, 495–509, doi:10.1002/2014PA002758.

Suan, G., Schöllhorn, I., Schlögl, J., Segit, T., Mattioli, E., Lécuyer, C., Fourel, F., Mattioli, E., 2018. Euxinic conditions and high sulfur burial near the European shelf margin (Pieniny Klippen Belt, Slovakia) during the Toarcian oceanic anoxic event. *Glob. Planet. Chang*. **170**, 246–259.

Tang J., Dietzel M., Böhm F., Köhler S. J. and Eisenhauer A. 2008. Sr^{2+}/Ca^{2+} and $^{44}Ca/^{40}Ca$ fractionation during inorganic calcite formation: II. Ca isotopes. *Geochim. Cosmochim. Acta*, **72**, 3733–3745.

Thibault N., Ruhl M., Ullmann C.V., Korte C., Kemp D.B., Gröcke D.R. and Hesselbo S.P. 2018. The wider context of the Lower Jurassic Toarcian oceanic anoxic event in Yorkshire coastal outcrops, UK. Proc. Geol. Assoc. **129**, 372–391.

Thierry J. and Barrier E. 2000. Middle Toarcian. *In*: Atlas Peri-Tethys. Palaeogeographical Maps. Dercourt, J., Gaetani, M.E.A J. Dercourt, M. Gaetani, B. Vrielynck, E. Barrier, B. Biju-Duval, M.F. Brunet, J.P. Cadet, S. Crasquin and M. Sandulescu (Editors), Paris.

Trecalli A., Spangenberg J., Adatte T., Föllmi K.B. and Parente M. 2012. Carbonate platform evidence of ocean acidification at the onset of the early Toarcian oceanic anoxic event. *Earth and Planetary Science Letters*, **357/358**, 214–225.

Uchikawa J. and Zeebe R.E. 2012. The effect of carbonic anhydrase on the kinetics and equilibrium of the oxygen isotope exchange in the CO_2–H_2O system: implications for $\delta^{18}O$ vital effects in biogenic carbonates. *Geochim. Cosmochim Acta*, **95**, 15–34.

Ullmann C.V. and Pogge von Strandmann P.A.E. 2017. The effect of shell secretion rate on Mg/Ca and Sr/ Ca ratios in biogenic calcite as observed in a belemnite rostrum. *Biogeosciences*, **14**, 89–97.

van Acken D, Tütken T., Daly J.S., Schmid-Röhl A. and Orr P.J. 2019. Rhenium‑osmium geochronology of the Toarcian Posidonia Shale, SW Germany *Palaeogeography, Palaeoclimatology, Palaeoecology*, **534**. 109294.

van de Schootbrugge, B., McArthur, J.M., Bailey, T.R., Rosenthal, Y., Wright, J.D., Miller, K.G., 2005. Toarcian oceanic anoxic event: an assessment of global causes using belemnite C isotope records. *Paleoceanography*, **20**, PA3008.

van de Schootbrugge B., Bachan A., Suan G., Richoz S., Payne J.L. 2013. Microbes, mud and methane: cause and consequence of recurrent early Jurassic anoxia following the end-triassic mass extinction. *Palaeontology*, **56(4)**, 685–709.

Vollstaedt H., Eisenhauer A., Wallmann K., Böhm F., Fietzke J., Liebetrau V., Krabbenhöft A., Farkaš J., Tomašých A., Raddatz J. and Veizer J. 2014. The Phanerozoic $\delta^{88/86}Sr$ record of seawater: new constraints on past changes in oceanic carbonate fluxes. *Geochimica et*

Cosmochimica Acta, **128**, 249–26.

von Allmen K., Nägler T.F., Pettke T., Hippler D., Griesshaber E., Logan A., Eisenhauer A. and Samankassou E. 2010.Stable isotope profiles (Ca, O, C) through modern brachiopod shells of *T. septentrionalis* and *G. vitreus*: implications for calcium isotope paleo-ocean chemistry. *Chemical Geology*, **269**, 210–219.

Wang J., Jacobson A.D., Zhang H., Ramezani J., Sageman B.B., Hurtgen M.T., Bowring S.A., Shen S.-Z. 2019. Coupled $\delta^{44}/^{40}$Ca, $\delta^{88}/^{86}$Sr, and ^{87}Sr/^{86}Sr geochemistry across the end-Permian mass extinction event. *Geochimica et Cosmochimica Acta*, **262**, 143–165.

Watkins J.M., Nielsen L/C.., Ryerson F.J. and DePaolo D.J. 2013. The influence of kinetics on the oxygen isotope composition of calcium carbonate. *Earth Planet. Sci. Letters*, **375**, 349–360.

Wignall, P.B., Newton, R.J. and Little, C.T.S. 2005. The timing of paleoenvironmental change and cause-and-effect relationships during the Early Jurassic mass extinction in Europe. *Am. J. Sci*. **305**, 1014–1032.

Xu W., Ruhl M., Jenkyns H.C., Hesselbo S.P., Riding J.B., Selby D., Naafs B.D.A., Weijers J.W.H., Pancost R.D., Tegelaar E.W. and Idiz E.F. 2017. Carbon sequestration in an expanded lake system during the Toarcian Oceanic Anoxic Event. *Nat. Geosci.* **10**, 129–134.

Xu W. Ruhl M., Jenkyns H.C., Leng M.J., Huggett J.M., Minisini D., Ullmann C.V. Riding J.B., Weijers J.W.H., Storm M.S., Percival L.M.E., Tosca N.J., Idiz E.F., Tegelaar E.W. and Hesselbo S.P. (2018). Evolution of the Toarcian (Early Jurassic) carbon-cycle and global climatic controls on local sedimentary processes (Cardigan Bay Basin,UK) *Earth Planet. Sci. Lett.*, **484**, 396–411.

List of Tables

Table 1. Elemental and isotopic compositions of belemnites and brachiopods analysed for this study. For $\delta^{44/40}$Ca measurements, R = RHUL, C= Cambridge, For locality, Y = Yorkshire, P = Peniche, For taxonomy, M = Megateuthididae, H = Hastites, P = Passaloteuthididae, B = Brachiopod. Measured $\delta^{44/40}Ca_{calcite}$ to SRM 951a; measured $\delta^{88/86}Sr_{calcite}$ to SRM 987. Base values are measured values corrected for natural isotopic fractionation on precipitation of calcite from seawater. Temperature from equation of Hayes and Grossman (1991).

List of Figures.

Fig. 1. Map showing the positions of the sections sampled in relation to the disposition of land masses across NW Europe during Early Toarcian time. Modified from Suan *et al.* (2018) after maps by Dera *et al.* (2009) and Thierry and Barrier (2000).

Fig. 2. Stratigraphy of the sections sampled in Peniche, Portugal, and Yorkshire, UK. Arrows denote the inception, development, and retreat of the driving force for the negative shift in $\delta^{13}C_{org}$ and euxinia in Yorkshire. Dysoxia in Peniche retreated before euxinia retreated from Yorkshire, whilst the C-isotope profiles are similar in both. The samples from Yorkshire are correlated to equivalent levels in Peniche using Sr-, C- and O-isotope stratigraphy (McArthur *et al.* 2000, 2020). Values of $\delta^{13}C_{bulk\ carb}$ in Peniche from Hesselbo *et al.* (2007) and values of $\delta^{13}C_{org}$ in Yorkshire from Kemp *et al.* (2005). Zone 1–3 based on Thibault *et al.* 2018.

Fig. 3. Correlations of base-$\delta^{44/40}Ca_{cal}$ to **a**) temperature for all samples. Temperatures are derived from $\delta^{18}O$ using the palaeo-temperature equation of Hays and Grossman (1991), and a value of −1 ‰ for $\delta^{18}O_{sw}$. **b**) Mg/Ca for belemnites and, **c)** plot of Sr/Ca, all samples.

Fig. 4. Base-$\delta^{88/86}Sr_{cal}$ does not correlate with either **a**) temperature or **b**) Sr/Ca.

Fig. 5. Profiles of $\delta^{44/40}Ca_{cal}$ through the studied sections: **a)** base-$^{44/40}Ca_{cal}$ **b)** base-$\delta^{44/40}Ca_{cal}$ corrected to 15°C, with temperature calculated from $\delta^{18}O_{cal}$, a seawater of $\delta^{18}O$ = −1 ‰, and the temperature dependency on fractionation of +0.020 ‰/°C (Fig. 3a). Also shown are the data of Brazier *et al.* (2015) corrected to 15°C; **c)** detrended-$\delta^{44/40}Ca_{cal}$ (corrected Mg/Ca = 11.5 mM/M). Values of $\delta^{13}C_{cal}$ from this work, with additional data for Peniche from Hesselbo *et al.* (2007). Values of $\delta^{13}C_{org}$ in Yorkshire from Kemp *et al.* (2005).

Fig. 6. Profile of $\delta^{88/86}Sr_{sw}$ through the sections at Peniche, Portugal, and Yorkshire, UK. The samples from Yorkshire are correlated to equivalent levels in Peniche using Sr-, C- and O-isotope stratigraphy (McArthur *et al.* 2000, 2020). Other data sources as in Fig. 6.

Fig. 7. Variations by $\delta^{44/40}Ca$ in seawater and $\delta^{13}C$ in carbonate sediment as a consequence of variations in three driving factors, as modelled by Silva-Tamayo *et al.* (2018).

Fig. 8. Profiles of $\delta^{11}B$ in brachiopod calcite from Peniche; data from Muller *et al.* (2020), corrected for contamination from clays (see Supplementary Information). Blue vertical lines is drawn at the mean values of corrected $\delta^{11}B$ and has a width equal to analytical uncertainty, calculated as the mean deviation from the means of 10 analyses of 5 pairs of samples from 5 different levels (mean = 0.39 ‰, n = 5).

Figure 1

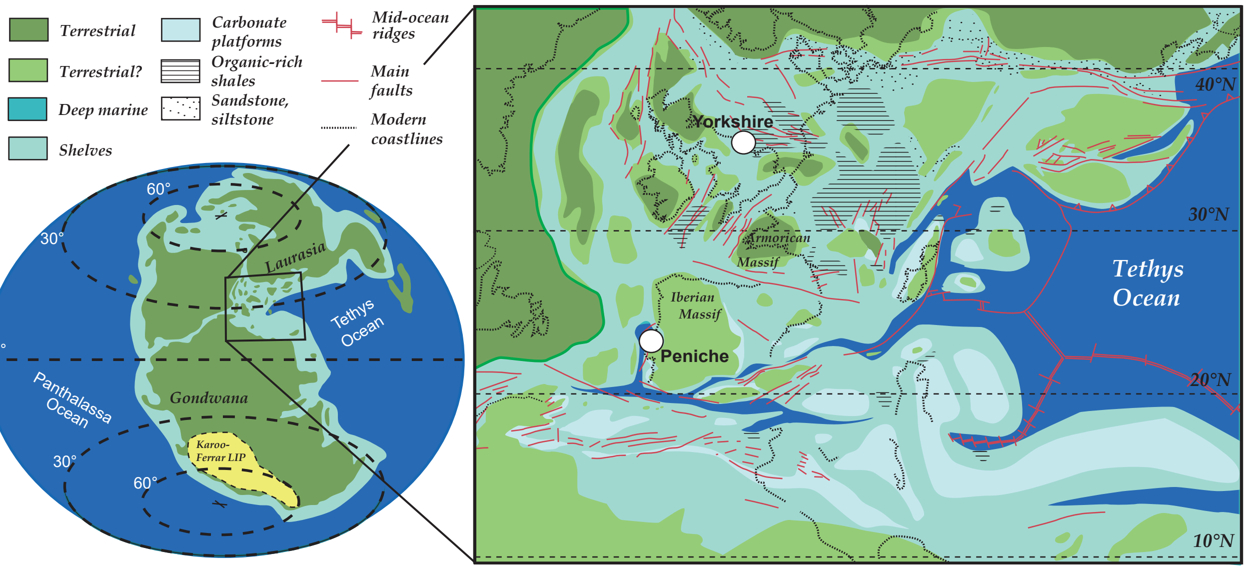
Terrestrial
Terrestrial?
Deep marine
Shelves
Carbonate platforms
Organic-rich shales
Sandstone, siltstone
Mid-ocean ridges
Main faults
Modern coastlines
60°
30°
0°
30°
60°
Laurasia
Tethys Ocean
Panthalassa Ocean
Gondwana
Karoo-Ferrar LIP
40°N
30°N
20°N
10°N
Yorkshire
Armorican Massif
Iberian Massif
Peniche
Tethys Ocean

Figure 2

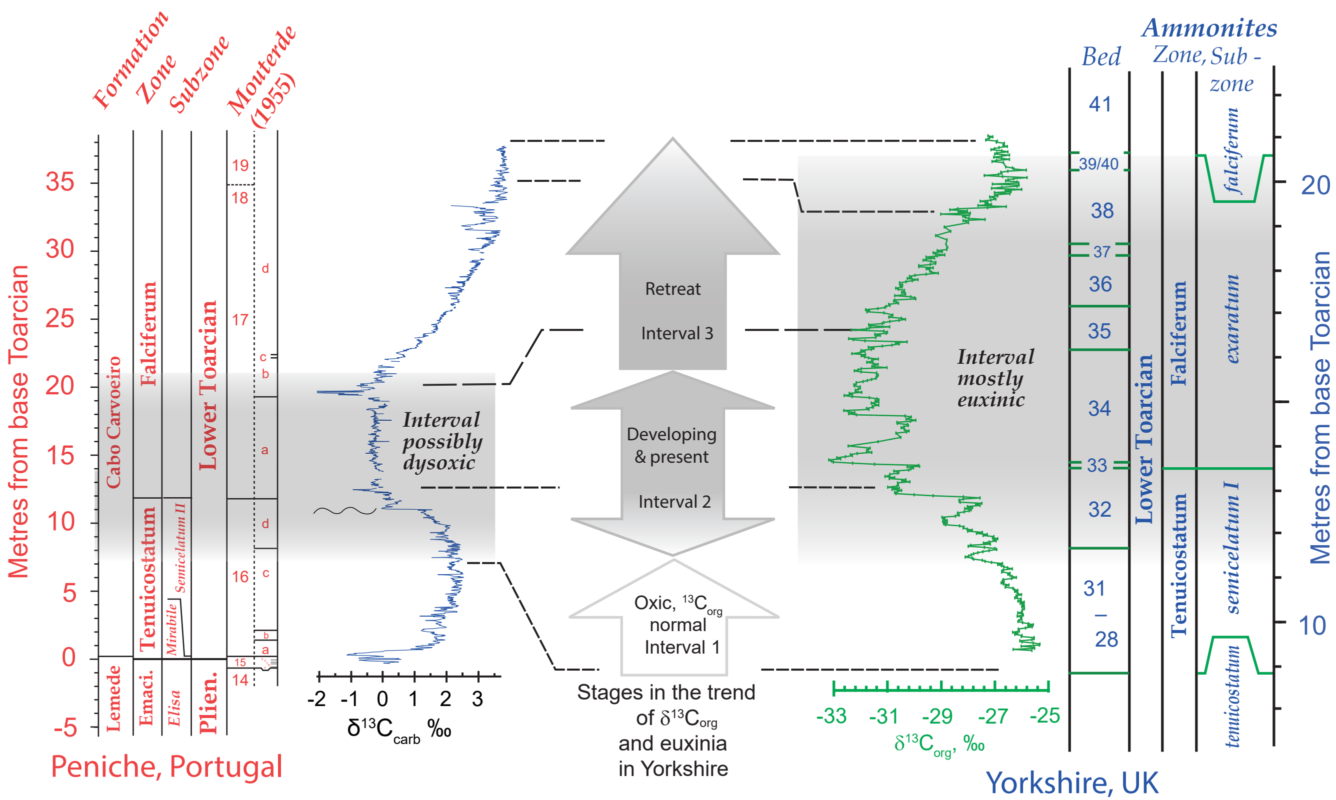

Formation
Zone
Subzone
Mouterde (1955)
Metres from base Toarcian
Cabo Carvoeiro
Lemede
Falciferum
Tenuicostatum
Emaci.
Semicelatum II
Mirabile
Elisa
Lower Toarcian
Plien.
Interval possibly dysoxic
δ13Ccarb ‰
Peniche, Portugal
Retreat
Interval 3
Developing & present
Interval 2
Oxic, 13Corg normal
Interval 1
Stages in the trend of δ13Corg and euxinia in Yorkshire
Interval mostly euxinic
δ13Corg, ‰
Bed
Ammonites
Zone, Sub - zone
falciferum
exaratum
semicelatum I
tenuicostatum
Metres from base Toarcian
Yorkshire, UK

Figure 3

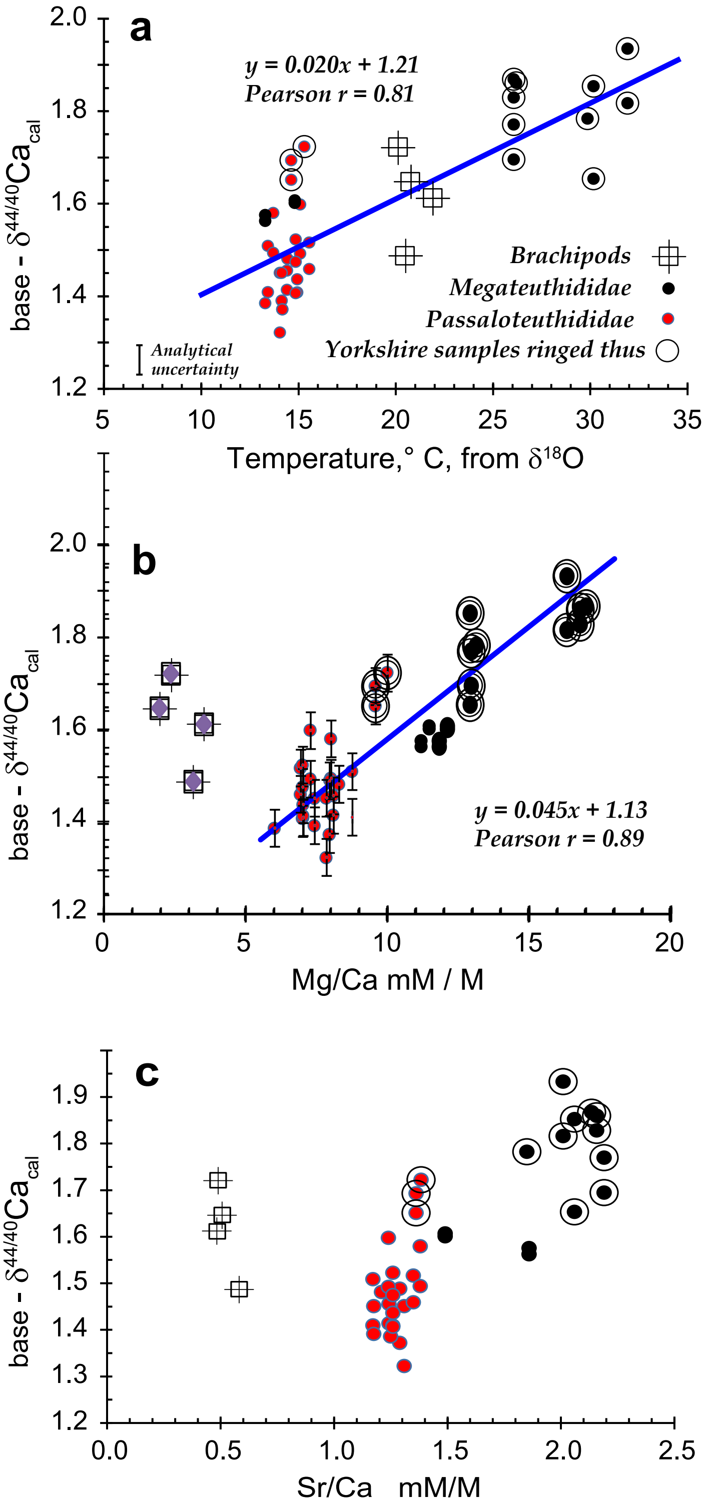

a
y = 0.020x + 1.21
Pearson r = 0.81
Brachipods
Megateuthididae
Passaloteuthididae
Yorkshire samples ringed thus
Analytical uncertainty
base - δ44/40Cacal
Temperature,° C, from δ18O
b
y = 0.045x + 1.13
Pearson r = 0.89
Mg/Ca mM / M
c
Sr/Ca mM/M

Figure 4

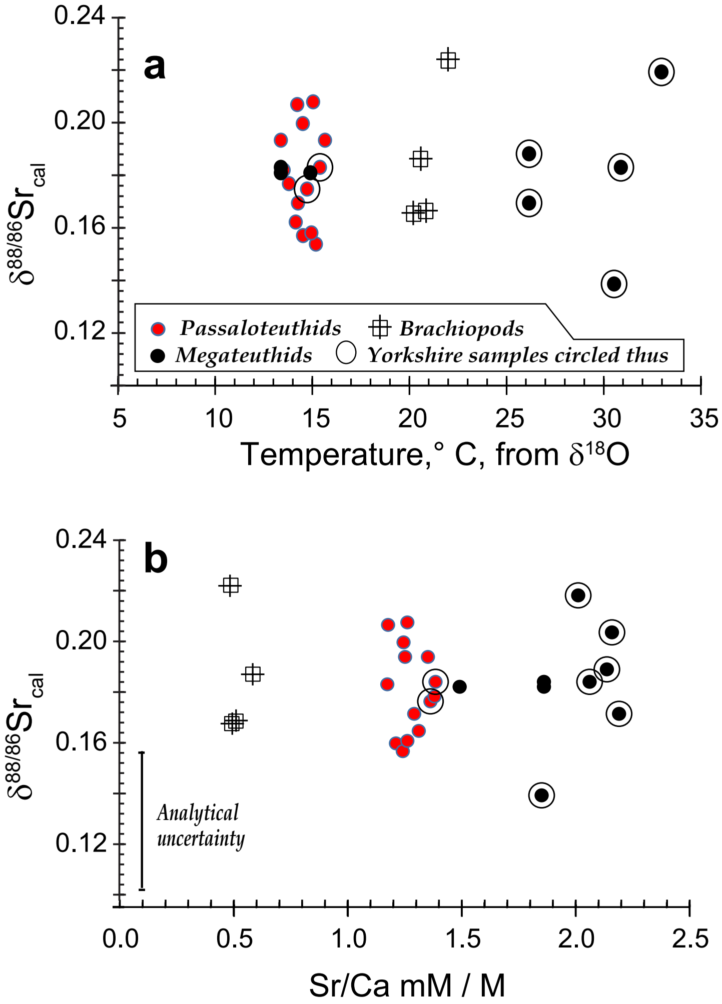

a
0.24
0.20
0.16
0.12
$\delta^{88/86}Sr_{cal}$
Passaloteuthids
Brachiopods
Megateuthids
Yorkshire samples circled thus
5
10
15
20
25
30
35
Temperature, ° C, from $\delta^{18}O$
b
0.24
0.20
0.16
0.12
$\delta^{88/86}Sr_{cal}$
Analytical uncertainty
0.0
0.5
1.0
1.5
2.0
2.5
Sr/Ca mM / M

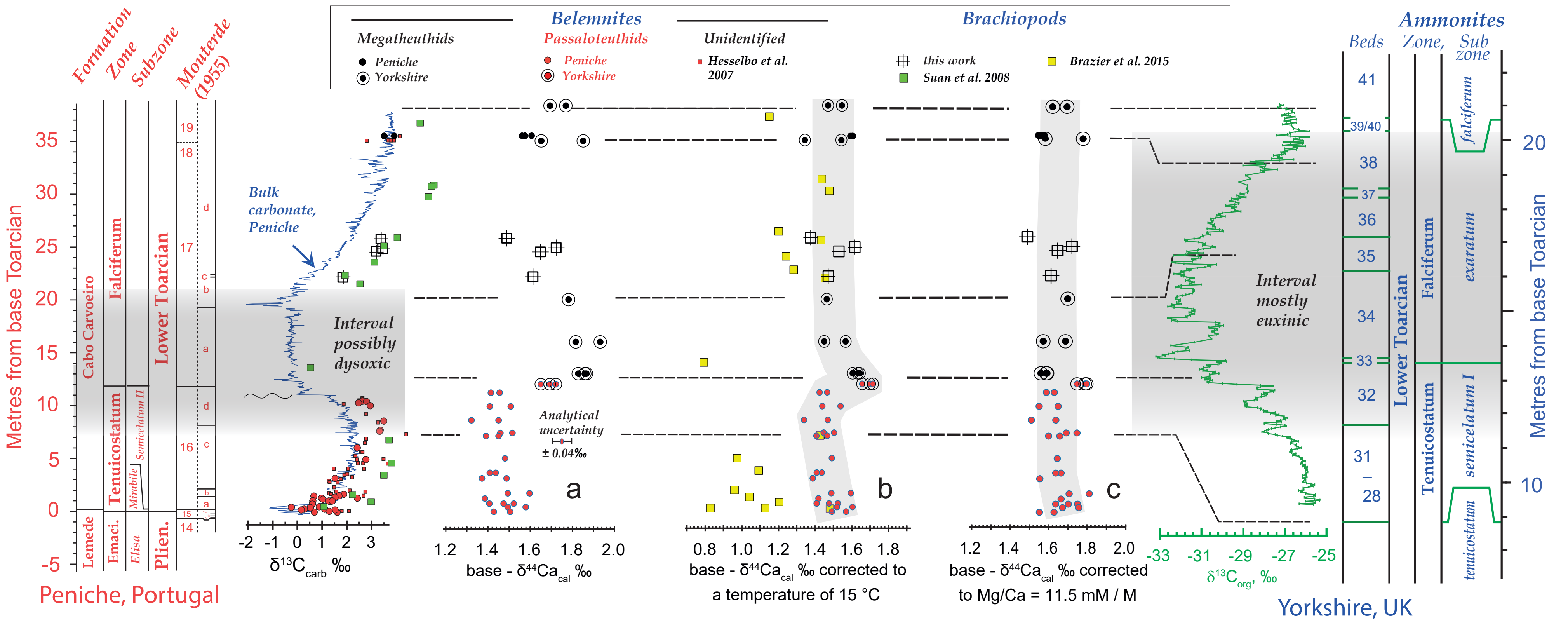
Belemnites
Megatheuthids
Peniche
Yorkshire
Passaloteuthids
Peniche
Yorkshire
Unidentified
Hesselbo et al. 2007
Brachiopods
this work
Suan et al. 2008
Brazier et al. 2015
Formation
Zone
Subzone
Mouterde (1955)
Metres from base Toarcian
Cabo Carvoeiro
Lemede
Falciferum
Tenuicostatum
Emaci.
Semicelatum II
Mirabile
Elisa
Lower Toarcian
Plien.
Bulk carbonate, Peniche
Interval possibly dysoxic
$\delta^{13}C_{carb}$ ‰
Analytical uncertainty ± 0.04‰
a
base - $\delta^{44}Ca_{cal}$ ‰
b
base - $\delta^{44}Ca_{cal}$ ‰ corrected to a temperature of 15 °C
c
base - $\delta^{44}Ca_{cal}$ ‰ corrected to Mg/Ca = 11.5 mM / M
Interval mostly euxinic
$\delta^{13}C_{org}$, ‰
Peniche, Portugal
Beds
Ammonites
Zone,
Sub zone
falciferum
exaratum
semicelatum I
tenuicostatum
Yorkshire, UK

Figure 6

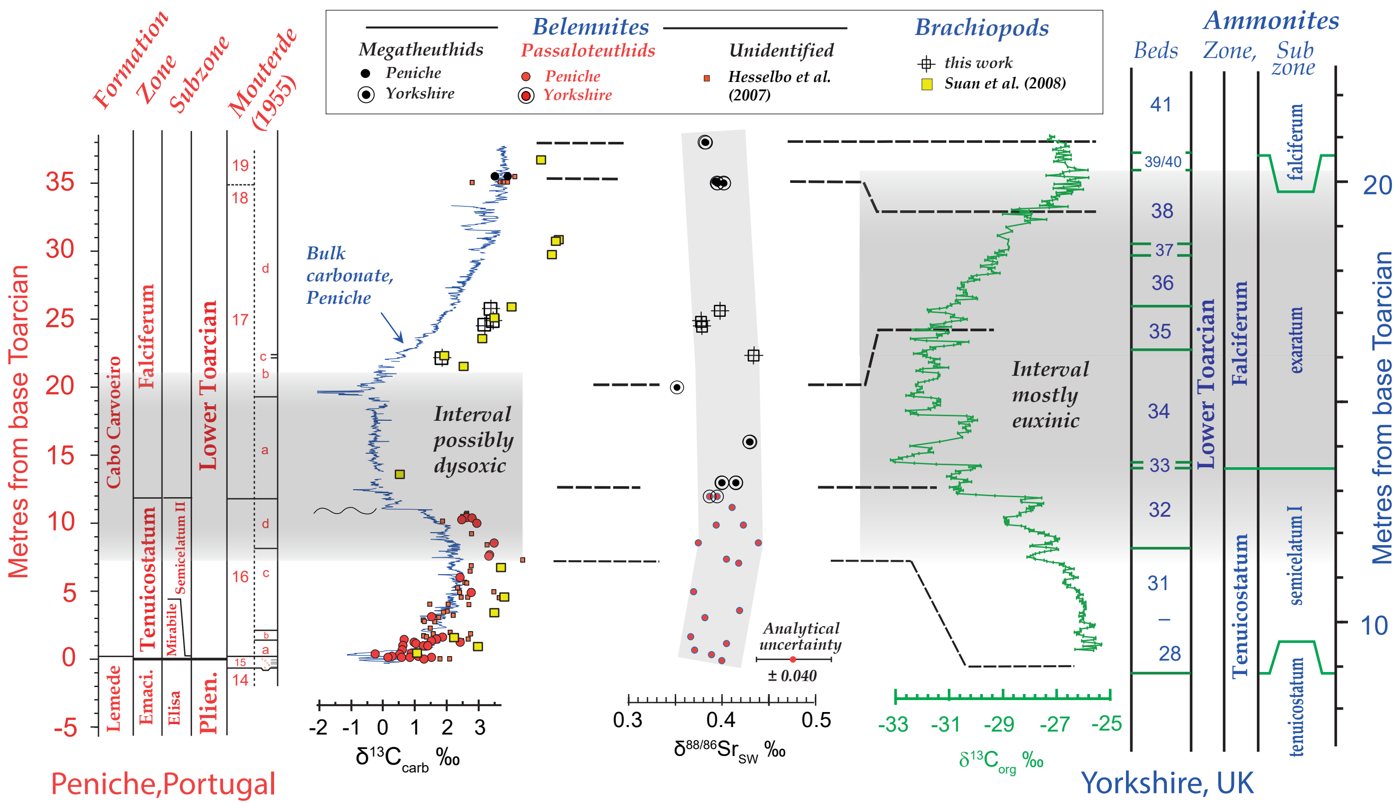

Formation
Zone
Subzone
Mouterde (1955)
Metres from base Toarcian
Cabo Carvoeiro
Lemede
Falciferum
Tenuicostatum
Emaci.
Semicelatum II
Mirabile
Elisa
Lower Toarcian
Plien.
Peniche,Portugal
Belemnites
Megatheuthids
Peniche
Yorkshire
Passaloteuthids
Peniche
Yorkshire
Unidentified
Hesselbo et al. (2007)
Brachiopods
this work
Suan et al. (2008)
Bulk carbonate, Peniche
Interval possibly dysoxic
$\delta^{13}C_{carb}$ ‰
Analytical uncertainty
± 0.040
$\delta^{88/86}Sr_{SW}$ ‰
Interval mostly euxinic
$\delta^{13}C_{org}$ ‰
Ammonites
Beds
Zone,
Sub zone
falciferum
exaratum
semicelatum I
tenuicostatum
Lower Toarcian
Falciferum
Tenuicostatum
Metres from base Toarcian
Yorkshire, UK

Figure 7

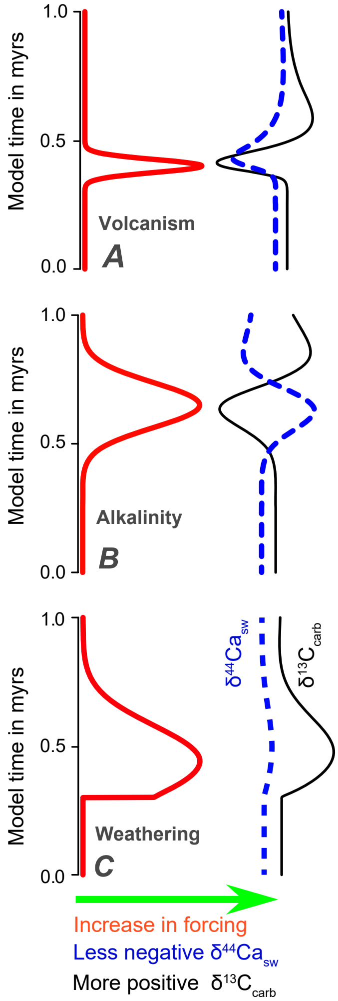
1.0
0.5
0.0
Model time in myrs
Volcanism
A
Alkalinity
B
Weathering
C
δ44Ca sw
δ13C carb
Increase in forcing
Less negative δ44Ca sw
More positive δ13C carb

Figure 8

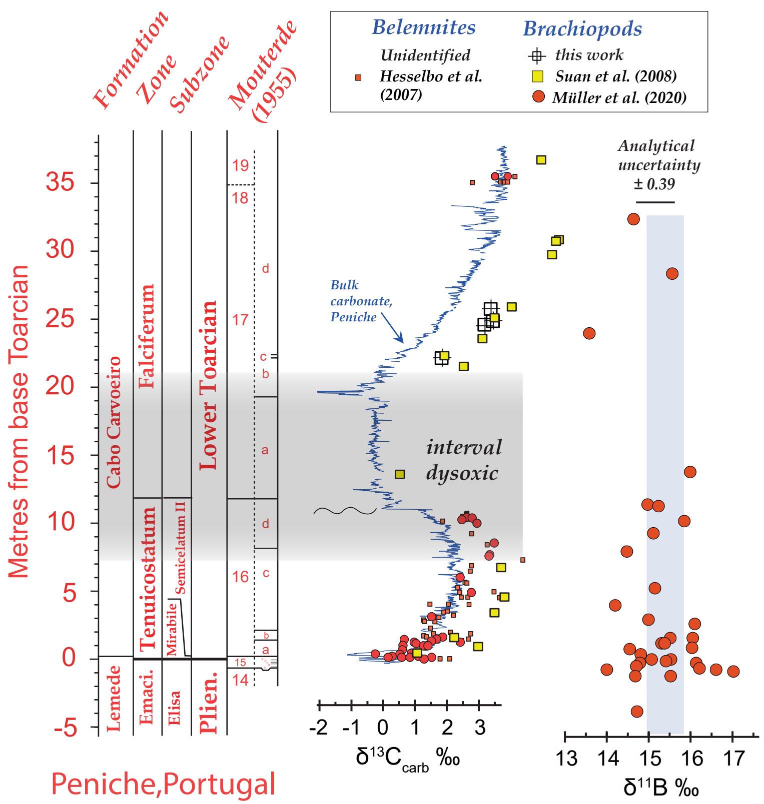

Formation
Zone
Subzone
Mouterde (1955)
Belemnites
Unidentified
Hesselbo et al. (2007)
Brachiopods
this work
Suan et al. (2008)
Müller et al. (2020)
Metres from base Toarcian
Cabo Carvoeiro
Falciferum
Lower Toarcian
Tenuicostatum
Semicelatum II
Mirabile
Lemede
Emaci.
Elisa
Plien.
Bulk carbonate, Peniche
interval dysoxic
Analytical uncertainty ± 0.39
δ13Ccarb ‰
δ11B ‰
Peniche,Portugal

Table 1

Stage	Ammonite Zone	Ammonite Subzone	Sample No and Bed No.	Taxa	Site	Specimen identification: belemnites unless indicated otherwise	Stratig. Level, m.a.d Peniche	Zone	Lab	Measured $\delta^{44/40}$Ca Calcite to 915a	± 2 s.e.	Base- $\delta^{44/40}$Ca Calcite to 915a	T-corr. $\delta^{44/40}$Ca Calcite to 915a	Detrend $\delta^{44/40}$Ca Calcite to 915a	Measured $\delta^{88/86}$Sr Calcite SRM 987	± 2 s.e.
Toarcian	Serpentinum	Exaratum Sz	PM 13	M	Y	?*Acrocoelites inaeqistriatus*	38.0	Zone 3	C	0.37	0.021	1.77	1.53	1.70	0.171	0.020
Toarcian	Serpentinum	Exaratum Sz	PM 13 Repeat				38.0	Zone 3		0.29	0.022	1.69	1.46	1.63		
Toarcian	Serpentinum		133A	M	P	Acrocoelites sp	35.1	Zone 3	C	0.17	0.030	1.58	1.61	1.59	0.182	0.025
Toarcian	Serpentinum		133A Repeat				35.1	Zone 3		0.16	0.022	1.56	1.60	1.58	0.184	0.034
Toarcian	Serpentinum		133B	M	P	Indet.	35.1	Zone 3	C	0.20	0.019	1.60	1.60	1.60	0.182	0.018
Toarcian	Serpentinum		133B Repeat				35.1	Zone 3		0.20	0.027	1.61	1.61	1.61		
Toarcian	Serpentinum	Exaratum Sz	Y18/PM/38(127/152)	M	Y	Acrocoelites sp	35.0	Zone 3	C	0.45	0.021	1.85	1.53	1.79	0.184	0.020
Toarcian	Serpentinum	Exaratum Sz	Y18/PM/38(127/152) Repeat				35.0	Zone 3		0.25	0.021	1.65	1.33	1.59	0.191	0.036
Toarcian	Serpentinum		13.3 m	B	P	*S. bouchardi* ?	25.8	Zone 3	C	0.64	0.022	1.49	1.37		0.187	0.040
Toarcian	Serpentinum		12.4 m	B	P	*S. bouchardi* ?	24.9	Zone 3	C	0.87	0.018	1.72	1.61		0.167	0.029
Toarcian	Serpentinum		12.0 m	B	P	*S. bouchardi* ?	24.5	Zone 3	C	0.80	0.021	1.65	1.52		0.168	0.031
Toarcian	Serpentinum		9.65 m	B	P	*S. bouchardi* ?	22.2	Zone 3	C	0.76	0.021	1.61	1.46		0.223	0.030
Toarcian	Serpentinum	Exaratum Sz	Y18/PM/35(0/91)	M	Y	Acrocoelites sp	20.0	Zone 2	C	0.38	0.020	1.78	1.47	1.71	0.139	0.028
Toarcian	Serpentinum	Exaratum Sz	Y18/PM/34(173/259)	M	Y	Acrocoelites sp	16.0	Zone 2	C	0.53	0.020	1.93	1.57	1.72	0.219	0.022
Toarcian	Serpentinum	Exaratum Sz	Y18/PM/34(173/259) Repeat				16.0	Zone 2		0.41	0.020	1.82	1.46	1.60		
Toarcian	Serpentinum	Semicelatum I	PM 106	M	Y	Acrocoelites sp	13.0	Zone 2	C	0.46	0.027	1.87	1.63	1.62	0.189	0.021
Toarcian	Serpentinum	Semicelatum I	PM 106 Repeat				13.0	Zone 2		0.43	0.024	1.83	1.59	1.59	0.204	0.019
Toarcian	Serpentinum	Semicelatum I	PM 106 Repeat 2				13.0	Zone 2		0.46	0.028	1.86	1.62	1.62		
Toarcian	Serpentinum	Semicelatum I	Y18/KS/32(138/183)	P	Y	*cf. Pseudohastites longiformis* (juv.)	12.0	Zone 2	C	0.29	0.021	1.69	1.70	1.78	0.176	0.019
Toarcian	Serpentinum	Semicelatum I	Y18/KS/32(138/183) Repeat				12.0	Zone 2		0.32	0.021	1.72	1.72	1.79	0.184	0.015
Toarcian	Serpentinum	Semicelatum I	Y18/KS/32(138/183) Repeat 2				12.0	Zone 2		0.25	0.032	1.65	1.66	1.74		
Toarcian	Tenuicostatum	Semicelatum II	25 B	P	P	Passaloteuthididae indet.	11.2	Zone 2	C	0.01	0.034	1.41	1.43	1.57	0.200	0.038
Toarcian	Tenuicostatum	Semicelatum II	25 B Repeat				11.2	Zone 2		0.05	0.034	1.46	1.47	1.61		
Toarcian	Tenuicostatum	Semicelatum II	24 Top	P	P	Passaloteuthididae indet.	9.90	Zone 2	C	0.11	0.023	1.51	1.54	1.63	0.183	0.028
Toarcian	Tenuicostatum	Semicelatum II	24 Top		P		9.90	Zone 2	R	0.01	0.051	1.41	1.44	1.53	0.212	0.028
Toarcian	Tenuicostatum	Semicelatum II	22 Mid	P?	P	Indet	8.60	Zone 2	C	-0.08	0.054	1.32	1.34	1.49	0.164	0.025
Toarcian	Tenuicostatum	Semicelatum II	22 Mid		P		8.60	Zone 2	R	0.05	0.091	1.45	1.47	1.61	0.228	0.035
Toarcian	Tenuicostatum	Semicelatum II	21B	P	P	*Passaloteuthis* sp. indet.	7.40	Zone 1	C	0.06	0.031	1.46	1.45	1.66	0.194	0.025
Toarcian	Tenuicostatum	Semicelatum II	21B		P		7.40	Zone 1	R	0.11	0.054	1.52	1.50	1.72		
Toarcian	Tenuicostatum	Semicelatum II	20	P	P	Passaloteuthididae indet.	7.10	Zone 1	C	0.05	0.031	1.45	1.47	1.63	0.207	0.025
Toarcian	Tenuicostatum	Semicelatum II	20		P		7.10	Zone 1	R	-0.01	0.057	1.39	1.41	1.57		
Toarcian	Tenuicostatum	Semicelatum II	17	P	P	Passaloteuthididae indet. juv.	5.00	Zone 1	C	0.08	0.022	1.48	1.49	1.62	0.159	0.029
Toarcian	Tenuicostatum	Semicelatum II	15	P?	P	Indet	3.63	Zone 1	C	0.03	0.042	1.44	1.44	1.64	0.208	0.021
Toarcian	Tenuicostatum	Semicelatum II	15		P		3.63	Zone 1	C	0.01	0.042	1.41	1.41	1.61		
Toarcian	Tenuicostatum	Semicelatum II	13 Top	P	P	*Passaloteuthis* sp. indet. juv.	3.10	Zone 1	C	-0.03	0.020	1.37	1.39	1.53	0.171	0.025
Toarcian	Tenuicostatum	Semicelatum II	13 Top		P		3.10	Zone 1	R	0.09	0.058	1.50	1.51	1.65		
Toarcian	Tenuicostatum	Semicelatum II	11 Mid	P	P	Passaloteuthididae indet. juv.	1.70	Zone 1	C	0.20	0.024	1.60	1.60	1.79	0.156	0.029
Toarcian	Tenuicostatum	Semicelatum II	11 Mid Repeat				1.70	Zone 1		0.09	0.020	1.49	1.49	1.68		
Toarcian	Tenuicostatum	Semicelatum II	7 Top	P	P	Passaloteuthididae indet.	1.20	Zone 1	C	-0.02	0.020	1.39	1.42	1.63	0.194	0.021
Toarcian	Tenuicostatum	Semicelatum II	3C	P	P	Passaloteuthididae indet.	0.72	Zone 1	C	0.00	0.025	1.41	1.41	1.61	0.160	0.025
Toarcian	Tenuicostatum	Semicelatum II	3C Repeat				0.72	Zone 1		0.12	0.038	1.52	1.52	1.72		
Toarcian	Tenuicostatum	Semicelatum II	3C		P		0.72	Zone 1	R	0.07	0.059	1.47	1.48	1.68		
Toarcian	Tenuicostatum	Semicelatum II	2	P?	P	?*Pseudohastites* sp. A	0.39	Zone 1	C	0.18	0.025	1.58	1.61	1.74	0.178	0.025
Toarcian	Tenuicostatum	Semicelatum II	2		P		0.39	Zone 1	R	0.09	0.060	1.49	1.52	1.65		
		Means, 2s.e.	**Zone 3 excluding brachs**										**1.535**	**1.636**	**0.182**	**0.0026**
		Means, 2s.e.	**Zone 3 incl brachs**										**1.521**		**0.184**	**0.0051**
		Means, 2s.e.	**Zone 2**										**1.540**	**1.640**	**0.191**	**0.0081**
		Means, 2s.e.	**Zone 1**										**1.477**	**1.654**	**0.181**	**0.0069**

$\delta^{88/86}$Sr	δ^{13}C	δ^{18}O	Temp	Ca	Mg	Sr	Ba	Na	Fe	Mn
Seawater	Cal.	Cal.	Cal.	Cal.	Cal.	Cal.	Cal.	Cal.	Cal.	Cal.
	‰V-PDB	‰V-PDB	°C	%	%	µg/g	µg/g	µg/g	µg/g	µg/g
		-1								
0.381	6.42	-3.30	26.4	38.9	0.305	1860	10	2678	31	4
0.392	3.93	-0.44	13.3	39.4	0.267	1601	4	1976	56	5
0.394										
0.392	3.51	-0.78	14.7	39.2	0.273	1275	5	1796	126	10
0.394	4.54	-4.22	31.0	39.2	0.307	1765	6	2542	46	7
0.401										
0.397	3.40	-2.05	20.4	41.2	0.079	524	1	446	89	19
0.377	3.47	-1.97	20.0	40.6	0.058	434	1	249	37	11
0.378	3.21	-2.11	20.7	40.8	0.048	453	1	262	52	13
0.433	1.87	-2.37	21.9	41.1	0.088	436	2	250	390	43
0.349	0.84	-4.15	30.6	39.2	0.312	1585	6	2033	26	2
0.429	1.22	-4.61	33.0	38.7	0.383	1700	17	2279	18	8
0.399	1.80	-3.30	26.4	38.3	0.395	1788	5	2130	7	8
0.414				37.9	0.386	1787				
0.386	2.72	-0.74	14.6	39.1	0.227	1164	12	1415	60	18
0.394	2.72	-0.89	15.2	39.7	0.241	1202				
	2.76	-0.74	14.6							
0.410	2.80	-0.69	14.4	40.1	0.197	1088	1	1240	11	2
				39.6	0.194	1076	2	673	32	5
0.393	2.95	-0.47	13.4	39.4	0.209	1009	1	1145	18	2
0.422										
0.374	3.49	-0.61	14.0	39.3	0.187	1126	1	1891	78	5
0.438										
0.404	3.35	-0.95	15.5	40.4	0.170	1193	1	1389	8	1
0.417	2.43	-0.63	14.1	39.6	0.179	1018	1	673	23	2
0.369	2.78	-0.70	14.4	39.6	0.199	1047	1	1400	80	4
0.418	2.32	-0.81	14.9	40.0	0.171	1101	1	1371	50	5
0.381	1.54	-0.64	14.1	40.0	0.193	1129	1	1313	22	2
0.366	1.88	-0.84	15.0	39.7	0.175	1076	1	1335	34	3
0.404	1.05	-0.44	13.3	40.2	0.147	1098	1	1100	2	1
0.370	0.62	-0.79	14.8	39.8	0.169	1096	5	917	20	2
				39.7	0.169	1092	1	588	29	2
0.388	0.54	-0.53	13.7	39.9	0.194	1205	1	1331	10	2
0.392										
0.394										
0.401										
0.391										